JPL Publication 88-21

A Comparison of Frequency Estimation Techniques for High-Dynamic Trajectories

V. A. Vilnrotter
S. Hinedi
R. Kumar

September 15, 1988

Prepared for

U.S. Air Force Systems Command
Armament Division

Through an agreement with

National Aeronautics and
Space Administration

by

Jet Propulsion Laboratory
California Institute of Technology
Pasadena, California

JPL Publication 88-21

A Comparison of Frequency Estimation Techniques for High-Dynamic Trajectories

V. A. Vilnrotter
S. Hinedi
R. Kumar

September 15, 1988

Prepared for

U.S. Air Force Systems Command
Armament Division

Through an agreement with

National Aeronautics and
Space Administration

by

Jet Propulsion Laboratory
California Institute of Technology
Pasadena, California

The research described in this publication was carried out by the Jet Propulsion Laboratory, California Institute of Technology, and was sponsored by the United States Air Force Systems Command, Armament Division through an agreement with the National Aeronautics and Space Administration.

ABSTRACT

This report presents a comparison of four different estimation techniques applied to the problem of continuously estimating the parameters of a sinusoidal Global Positioning System (GPS) signal, observed in the presence of additive noise, and under extremely high-dynamic conditions. Frequency estimates are emphasized, although phase and/or frequency rate are also estimated by some of the algorithms. These parameters are related to the velocity, position, and acceleration of the maneuvering transmitter. Estimated performance at low carrier-to-noise ratios and high dynamics is investigated for the purpose of determining the useful operating range of an approximate maximum likelihood (ML) estimator, an extended Kalman filter (EKF), a cross-product automatic frequency control (CPAFC) loop, and a digital phase-locked loop (PLL). Numerical simulations are used to evaluate performance while tracking a common trajectory exhibiting high dynamics.

ACKNOWLEDGMENTS

The authors would like to thank Leon Alvarez for implementing the extended Kalman filter, Unjeng Cheng for the phase-locked loop simulation, Joseph Statman for writing the trajectory simulation program, and William Hurd for guidance and encouragement throughout this effort.

CONTENTS

LIST OF FIGURES AND TABLES

I. INTRODUCTION

The problem of estimating the parameters of a single-frequency tone in the presence of additive noise occurs often in engineering. The parameters of interest are typically the tone's amplitude, phase, frequency and its time derivatives. Here our primary interest is in real-time estimation of dynamic doppler frequency, assuming constant amplitude. Estimation of the received phase is considered to be of secondary importance.

Accurate frequency estimation and tracking is of fundamental concern in the design of Global Positioning System (GPS) receivers observing signals that exhibit high dynamics. GPS receivers process radio signals received from a constellation of 18 satellites in order to determine the receiver's position and velocity. Each signal is the sum of two L-band carriers, biphase modulated by pseudorandom codes and information streams. We assume that the modulation is known and has been removed from the signal. This assumption is valid when the ground station establishes a direct link with the GPS satellites, in parallel with the link to the transponder aboard the maneuvering target. Decoded data from the direct link can then be used to wipe data from the transponder link, effectively transforming these signals into unmodulated RF tones. The problem then reduces to estimating the parameters of two sinusoidal signals in additive noise. Here we concentrate on one of these tones, namely the L1 carrier at a frequency of 1.575 GHz.

In a previous paper [1], an estimator structure based on the maximum likelihood estimator of code delay and doppler frequency over a single symbol interval was analyzed. At signal-to-noise ratios above 30 dB-Hz, this

estimator performed well in the presence of considerable acceleration and jerk, even though no attempt was made to compensate for the effects of these trajectory components. The estimation error was close to the Cramer-Rao bound above 30 dB-Hz, below which rapid performance deterioration occurred, leading to loss-of-lock at about 28 dB-Hz.

In the current application, the data have been removed from the carrier, hence we assume the estimator observes a sinusoid in the presence of additive noise. The frequency of the received sinusoid varies with time according to the trajectory of the vehicle being tracked. In principle, the estimator is free to observe the signal over several symbol intervals, thus decreasing both the estimation errors and the loss-of-lock threshold. However, rapid changes in the trajectory limit the maximum time interval during which the estimated parameters remain constant. Thus, a classical trade-off between noise suppression and doppler tracking results.

Four different estimation techniques will be compared in the following sections. First we consider an extension of the "approximate maximum likelihood" technique described in [1]. This technique involves a significant extension of previous results, hence it will be developed in some detail. Second, an extended Kalman filter with parameters matched to the dynamics of the signal is described and analyzed, again in some detail due to the novelty of the high-dynamic application. The third technique employs a cross-product frequency control loop to obtain frequency estimates. Finally, the fourth approach examines a standard digital phase-locked loop. In all cases, estimator performance is compared on the basis of root mean squared estimation error and probability of loss-of-lock, while tracking a common simulated high-dynamic trajectory.

This article is subdivided into six sections. Section II describes the common trajectory used in the simulations. Section III is devoted to the development of the appropriate signal and noise models. The estimation algorithms are described and analyzed in Section IV, and the simulation results are compared in Section V. Summary and conclusions are presented in Section VI. Finally, the Cramer-Rao bound on the estimation error for the case of unknown acceleration is derived in the Appendix.

II. COMMON TRAJECTORY

The performance of the various estimators is evaluated on the basis of their ability to track a common trajectory. The trajectory chosen for simulation consists of positive- and negative-going jerk pulses of 0.5-sec duration and magnitude of 100 g/sec, separated by two seconds of constant acceleration, as shown in Fig. 1(a). The corresponding acceleration and velocity trajectories are shown in Figs. 1(b) and 1(c). The initial conditions for acceleration were chosen for symmetric 25-g excursions. The velocity trajectory is converted to an equivalent doppler frequency trajectory as

$$f_d(t) = \left(\frac{f_c}{c}\right) v_d(t) \qquad \text{(Hz)} \tag{1}$$

which shows the one-to-one correspondence between the velocity $v_d(t)$ of the physical trajectory and the instantaneous frequency of the received signal. Here $v_d(t)$ is the doppler velocity, f_c denotes the carrier frequency, and c is the speed of light. Examination of Fig. 1(c) reveals that the doppler velocity, hence doppler frequency, of this trajectory can be well approximated by a piecewise linear model over time intervals on the order of 0.1 sec, even when a 100 g/sec jerk pulse is applied. This observation forms the basis for reducing the complexity of the simulated maximum likelihood estimator, as described in Section IV.

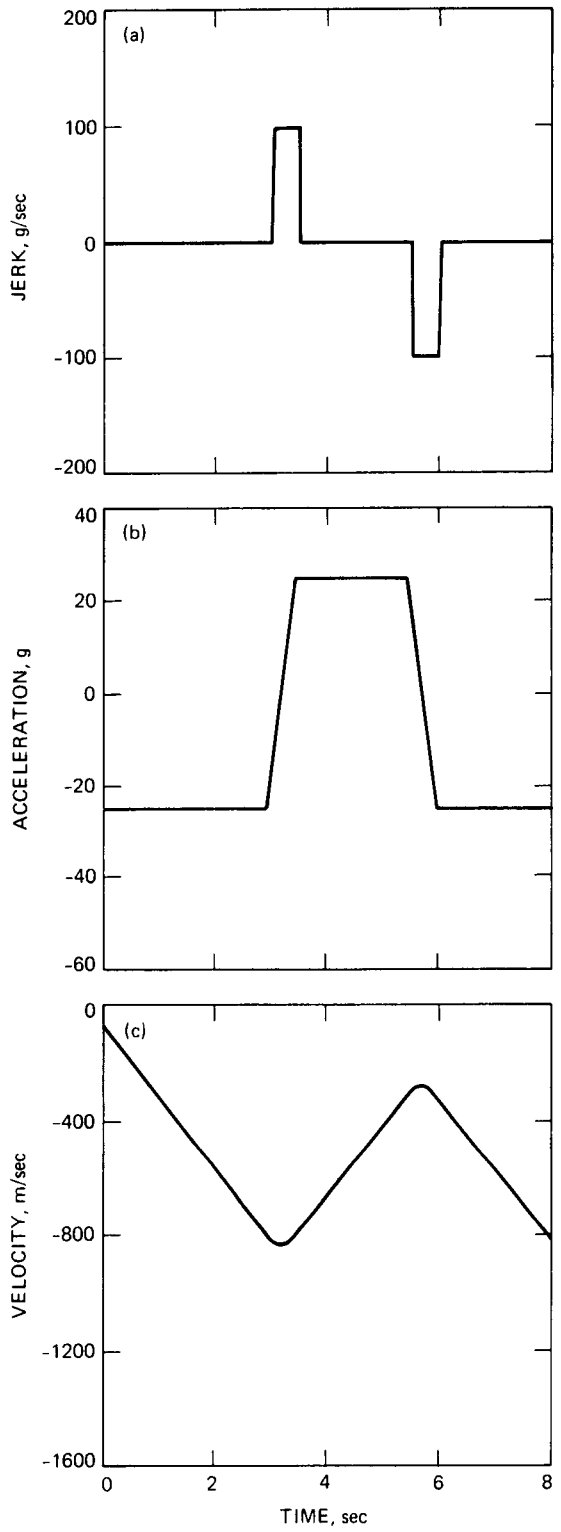

Figure 1. Simulated Trajectory

The common input to the simulation programs consists of samples of in-phase and quadrature sinusoids with phases proportional to the integral of the simulated frequency, plus independent additive noise samples. The properties of these input samples are easily derived from the continuous model of the received waveform. Therefore we begin by developing a suitable model for the trajectory-modulated received signal.

III. THE RECEIVED SIGNAL

In the absence of noise, the received signal at the antenna may be represented as

$$s(t) = \mathrm{Re}\left\{\sqrt{2}\ \tilde{s}(t)\ e^{j\omega_c t}\right\} \tag{2a}$$

$$\tilde{s}(t) = Ae^{j\theta(t)} \tag{2b}$$

where $\tilde{s}(t)$ is the signal complex envelope, A is its amplitude, $\omega_c = 2\pi f_c$, and where the phase process $\theta(t)$ is defined in terms of the doppler frequency process $f_d(t)$ as

$$\theta(t) = 2\pi \int_{-\infty}^{t} f_d(\zeta)\, d\zeta \tag{3}$$

This trajectory-modulated signal is observed in the presence of a zero mean, stationary, narrow-band Gaussian noise process n(t), with representation

$$n(t) = \mathrm{Re}\left\{\sqrt{2}\ \tilde{n}(t)\ e^{j\omega_c t}\right\} \tag{4}$$

where $\tilde{n}(t)$ is the complex envelope of the narrowband process. If the bandwidth of the noise process greatly exceeds that of the signal, then the covariance function of the complex envelope may be approximated as

$$K_{\tilde{n}}(\tau) \triangleq E[\tilde{n}(t+\tau)\ \tilde{n}^*(t)] \simeq N_0\delta(\tau) \tag{5}$$

where N_0 is the two-sided spectral level of $\tilde{n}(t)$. Henceforth, we assume that N_0 is known. One can show that the two-sided spectral level of the corresponding real bandpass process is $N_0/2$. In the current application,

the carrier is first removed by mixing the received signal with sinusoids at the carrier frequency, yielding in-phase and quadrature components. Typically, both the in-phase and quadrature signals are first sampled at a high rate (mega-samples per second), and subsequently input to digital accumulators. The output of the accumulators, viewed as complex samples, can be modeled as

$$\tilde{r}_i = T_s^{-1} \int_{iT_s}^{(i+1)T_s} \tilde{r}(t)\, dt = \tilde{s}_i + \tilde{n}_i \tag{6}$$

where $\tilde{r}(t) = \tilde{s}(t) + \tilde{n}(t)$ is the complex envelope of the received signal. In the subsequent simulations, the effective integration time, T_s, will be exactly 2 msec in duration. The effects of spectral roll-off due to the effective integration will be ignored in this paper. If T_s is short compared to the variation in $\tilde{s}(t)$, then by the mean-value theorem there exists a t_i in the i-th T_s interval such that $\tilde{s}_i = \tilde{s}(t_i)$. For suitably small T_s, we may regard t_i as the center of the i-th integration interval.

Derivation of noise sample statistics is straightforward. Since $\tilde{n}(t)$ is a complex zero mean Gaussian process, $\tilde{n}_i$ is a complex zero-mean random variable with covariance

$$E(\tilde{n}_i \tilde{n}_k^*) = (T_s)^{-2} \int_{iT_s}^{(i+1)T_s} dt_1 \int_{kT_s}^{(k+1)T_s} dt_2\, \overline{\tilde{n}(t_1)\, \tilde{n}^*(t_2)} = \frac{N_0}{T_s}\, \delta_{ik} \tag{7}$$

Here the overbar denotes the expectation operator, and δ_{ik} is the Kroenecker delta. Since all of the samples are pairwise uncorrelated, the joint density of any N distinct samples can be expressed as the product of the individual densities. This property is fundamental to much of our subsequent analysis.

IV. DESCRIPTION AND ANALYSIS

In this section, the various frequency estimation algorithms are described and analyzed. Some of the algorithms also provide useful phase estimates; however, we shall not address the phase tracking problem explicitly. Analytical expressions for estimator performance are obtained where possible. In all cases, estimator performance is evaluated by means of numerical simulations.

MAXIMUM LIKELIHOOD (ML) ESTIMATOR

The maximum likelihood (ML) estimates of the signal parameters are those values that simultaneously maximize the conditional joint probability density of the observation vector, conditioned on the signal parameters. If the statistical distribution of the signal parameters within some uncertainty interval is not known, then maximum likelihood estimation yields the smallest estimation error variance. For each estimate, the observation vector consists of consecutive samples obtained over a time interval that is short compared to the characteristic timescale of the trajectory variations. We begin by developing a representation for the received phase process.

Near a point t_0 in the domain of the trajectory function the frequency process can be represented in terms of a Taylor series expansion as

$$f_d(t)\Big|_{t=t_0} = \sum_{k=0}^{\infty} f_k \frac{(t - t_0)^k}{k!} \tag{8a}$$

$$f_k \triangleq \frac{\partial^k f(t)}{\partial t^k}\Big|_{t=t_0} \tag{8b}$$

This representation is valid where all derivatives exist. For the trajectory function illustrated in Fig. 1, we can let $f_k = 0$ for $k > 2$, everywhere except at the points of discontinuity. As an example, near the point $t_0 = 0$, representing the center of an observation interval,

$$\theta(t) = \theta_0 + 2\pi\left(f_0 t + \frac{f_1}{2} t^2 + \frac{f_2}{6} t^3\right) \tag{9}$$

The coefficient f_0 represents the doppler frequency in Hz, f_1 its first derivative with units of Hz/sec, and f_2 its second derivative with respect to time (Hz/sec^2). These coefficients correspond to the velocity, acceleration, and jerk of the physical trajectory. Henceforth we shall use the vector notation $\underline{f} = (f_0, f_1, f_2)$ to denote these signal parameters.

a. Maximum Likelihood Estimator Structure.

The maximum likelihood estimator uses the conditional probability density of the observable vector, conditioned on the parameters of interest. Since the signal in Eq. (2b) is completely specified by the parameters A, θ_0, and $\underline{f}$, it is equivalent to condition on the signal samples as

$$p(\tilde{\underline{r}}|\tilde{\underline{s}}) = \left(\frac{\pi N_0}{T_s}\right)^{-N} \exp\left[-\sum_{i=-N/2}^{(N/2)-1} |\tilde{r}_i - \tilde{s}_i|^2 \Big/ \left(\frac{N_0}{T_s}\right)\right] \quad ; \text{ N even} \tag{10}$$

The maximum likelihood estimates of the signal parameters are those values that simultaneously maximize this conditional joint density.

Equivalently, we can maximize any monotonically increasing functional of the conditional joint density, such as the logarithm. Taking the natural log of Eq. (10) and discarding terms which contain no information about the signal yields the "log-likelihood" function

$$\Lambda(\underline{\tilde{r}}) = \left(\frac{T_s}{N_0}\right)\left\{2\mathrm{Re}\left(\sum_{i=-N/2}^{(N/2)-1} \tilde{r}_i \tilde{s}_i^*\right) - \sum_{i=-N/2}^{(N/2)-1} |\tilde{s}_i|^2\right\} \tag{11}$$

Here $\underline{\tilde{r}}$ is an observation vector of length N, and $\tilde{r}_i$, $\tilde{s}_i$ are the samples defined in Eq. (6). With no loss in generality, the observation interval is assumed to be centered around the origin. Using Eq. (9) in Eq. (2b), we write the signal samples as

$$\tilde{s}_i = Ae^{j\theta_0} e^{jg_i(\underline{f})} \tag{12a}$$

$$g_i(\underline{f}) = 2\pi f_0 t_i + h_i(f_1, f_2) \tag{12b}$$

$$h_i(f_1, f_2) = 2\pi\left(\frac{f_1}{2} t_i^2 + \frac{f_2}{6} t_i^3\right) \tag{12c}$$

Substituting Eq. (12) into Eq. (11) yields

$$\Lambda(\underline{\tilde{r}}) = \left(\frac{T_s}{N_0}\right)\left\{2\mathrm{Re}\left[Ae^{-j\theta_0} \sum_{i=-N/2}^{(N/2)-1} \tilde{z}_i e^{-j2\pi f_0 t_i}\right] - NA^2\right\} \tag{13}$$

in terms of the modified samples $\tilde{z}_i \triangleq \tilde{r}_i \exp(-jh_i)$. This is the function to be maximized. Following the development in [1], we recall that for any

complex x, $\mathrm{Re}[\exp(-j\theta_0)x]$ is maximized with respect to θ_0 when $\theta_0 = \arg(x)$, taking on the value $|x|$. Thus,

$$\hat{\theta}_0 = \arg\left[\sum_i \tilde{z}_i e^{-j2\pi f_0 t_i}\right] \tag{14}$$

Substituting into Eq. (13) yields

$$\max_{\theta_0} \Lambda(\underline{\tilde{r}}) = \left(\frac{T_s}{N_0}\right)\left\{2A\left|\sum_i \tilde{z}_i e^{-j2\pi f_0 t_i}\right| - A^2 N\right\} \tag{15}$$

Since the amplitude is assumed to be unknown, its estimate $\hat{A}$ is found by differentiating Eq. (15) with respect to A, equating to zero and solving:

$$\hat{A} = \frac{1}{N}\left|\sum_i \tilde{z}_i e^{-j2\pi f_0 t_i}\right| \tag{16}$$

Using this value in Eq. (15) yields

$$\max_{r_0, A} \Lambda(\underline{\tilde{r}}) = \left(\frac{T_s}{N_0}\right) N^{-1}\left|\sum_i \tilde{z}_i e^{-j2\pi f_0 t_i}\right|^2 \tag{17}$$

Recalling that $\tilde{z}_i$ contains the desired parameters f_1 and f_2, it follows that the maximum likelihood estimates $(\hat{f}_0, \hat{f}_1, \hat{f}_2)$ are those values that simultaneously maximize Eq. (17). Letting $t_i = (i + (1/2))T_s$ and dividing by the constant coefficient, we can equivalently maximize

$$L(f_0, f_1, f_2) = \left|\sum_{i=-N/2}^{(N/2)-1} \tilde{z}_i e^{-j2\pi f_0 i T_s}\right|^2 \tag{18}$$

The function $L(f_0, f_1, f_2)$ is proportional to the squared magnitude of the Fourier transform of the modified sequence $\{\tilde{z}_i\}$. This interpretation is useful for implementation, since efficient FFT algorithms can be employed to carry out the maximization. In general, estimator complexity depends on the number of significant terms in the Taylor series expansion of the received phase, which in turn depends on the trajectory. Thus, there is a direct link between the trajectory and the effective dimensions of the maximum likelihood estimator.

b. Estimator Performance.

In the current application, estimation of the received frequency is emphasized. The other parameters are regarded as "nuisance parameters" which may nevertheless have to be estimated to achieve best performance. The estimates are typically subject to threshold effects characteristic of nonlinear estimators, which means that below some critical carrier-to-noise ratio (CNR $\triangleq A^2/N_0$) catastrophic deterioration in estimator performance begins to occur. Above threshold, estimator performance can be assessed by means of Cramer-Rao bounds. Below threshold, however, the breakdown mechanism must be modeled accurately to arrive at useful error estimates. We begin by developing some concepts that are necessary for understanding estimator performance.

The maximum likelihood estimates of frequency and its time derivatives are those values $\hat{f}_0$, $\hat{f}_1$, and $\hat{f}_2$ that simultaneously maximize the real

function $L(\underline{f})$. Let f'_{ℓ}, $\ell = 0,1,2$ denote the true parameter values, and let $G(\underline{\Delta f})$ denote the function

$$G(\underline{\Delta f}) = N^{-1} \sum_{i=-N/2}^{(N/2)-1} \exp\{-jg_i(\underline{\Delta f})\} \tag{19}$$

where $\Delta f_{\ell} = f_{\ell} - f'_{\ell}$, and $g_i(\underline{\Delta f})$ is defined in Eq. (12b). We observe that $|G(\underline{\Delta f})|^2$ is proportional to $L(\underline{f})$ centered over $\underline{f}'$ when the variance of the noise samples approaches zero. The projections of $|G(\underline{\Delta f})|^2$ onto cartesian coordinates defined by the signal parameters are shown in Figs. 2(a-c) where we let $G(\Delta f_0)$ denote $G(\Delta f_0,0,0)$, and so on. Note that the peak of the function $|G(\Delta f_{\ell})|^2$ always occurs at the true parameter values, and that its shape depends only on the deviation from the true value: the coordinates of the peak track the temporal variations in the signal parameters, while the shape of the function remains unchanged. Therefore at high CNR, we expect the estimates to be near the peak along each coordinate, and the estimation errors to be related to the main lobe dimensions.

The effects of acceleration and jerk errors on $|G(\Delta f_0)|^2$ are shown in Figs. 2(d-f). Evidently, acceleration errors result in decreased peak amplitude (Fig. 2(d)), whereas jerk errors give rise to a shift in the peak as well (Fig. 2(e)). Significantly reduced and shifted peak values can result when both acceleration and jerk errors are present simultaneously, as shown in Fig. 2(f).

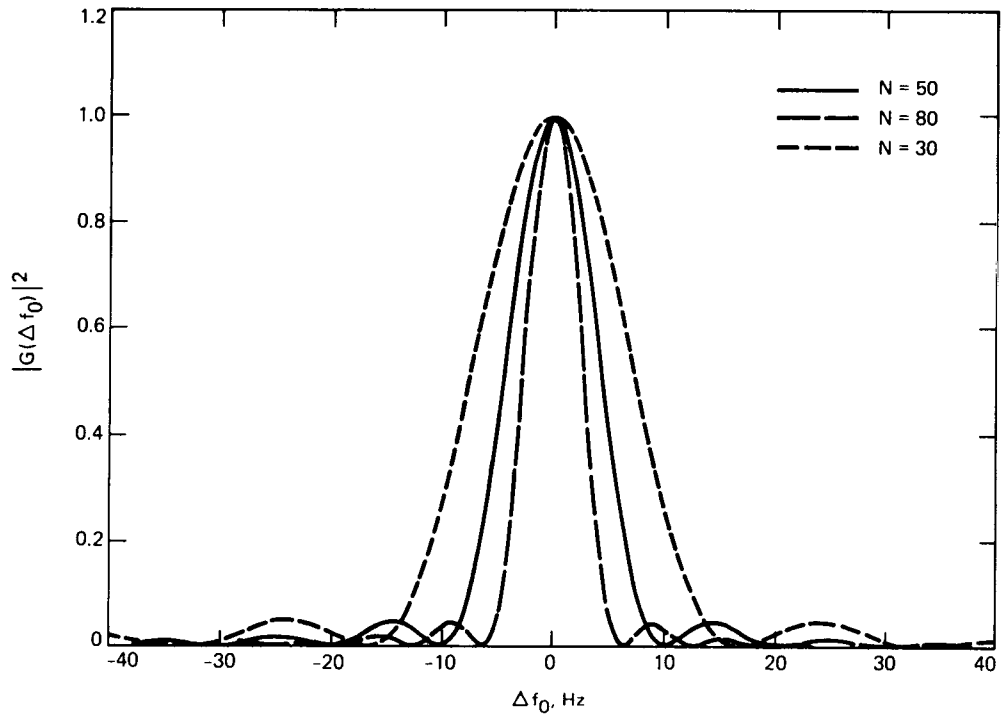

Figure 2(a). $|G(\Delta f_0)|^2$ as a Function of Deviation from the True Frequency

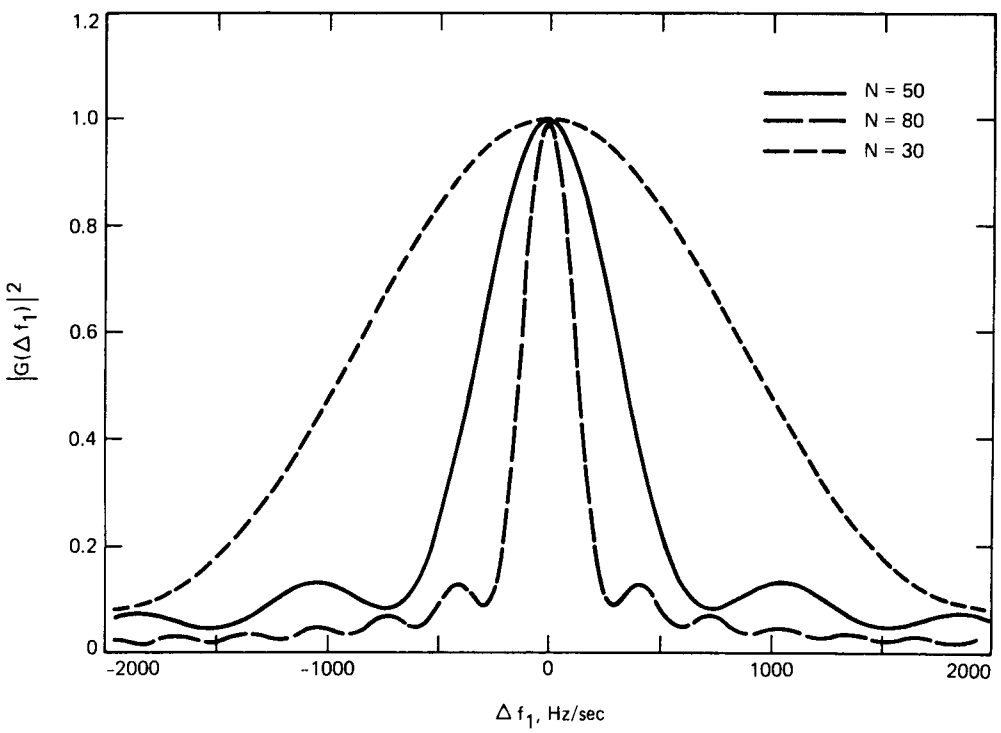

Figure 2(b). $|G(\Delta f_1)|^2$ as a Function of Deviation from the True Frequency Rate

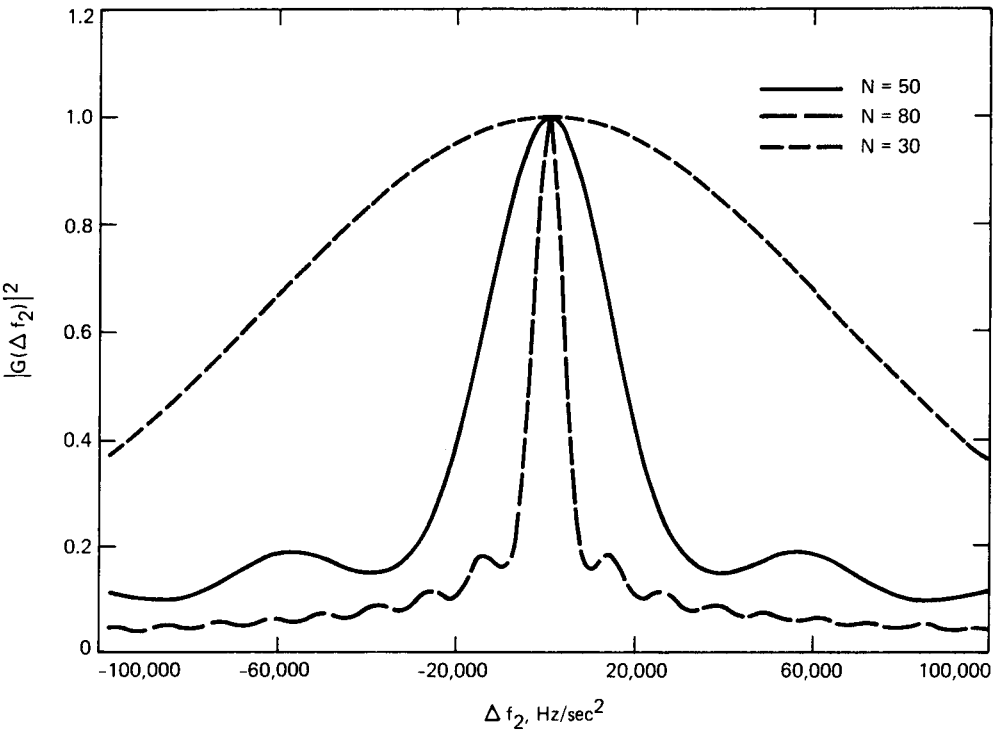

Figure 2(c). $|G(\Delta f_2)|^2$ as a Function of Deviation from the True Derivative of Frequency Rate

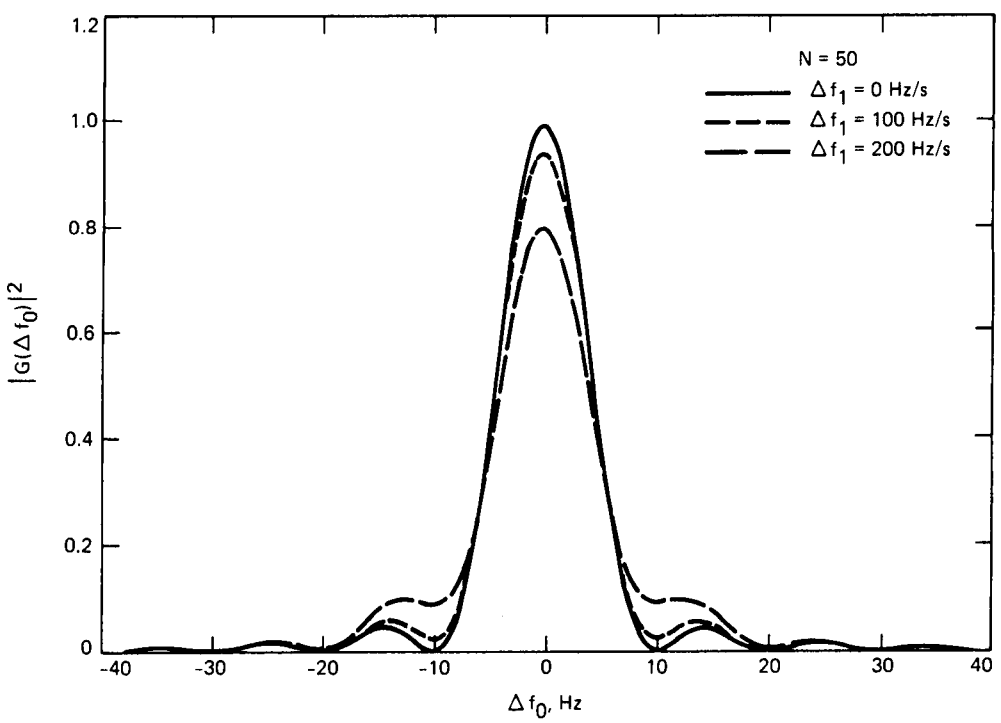

Figure 2(d). The Effect of Acceleration Error on $|G(\Delta f_0)|^2$

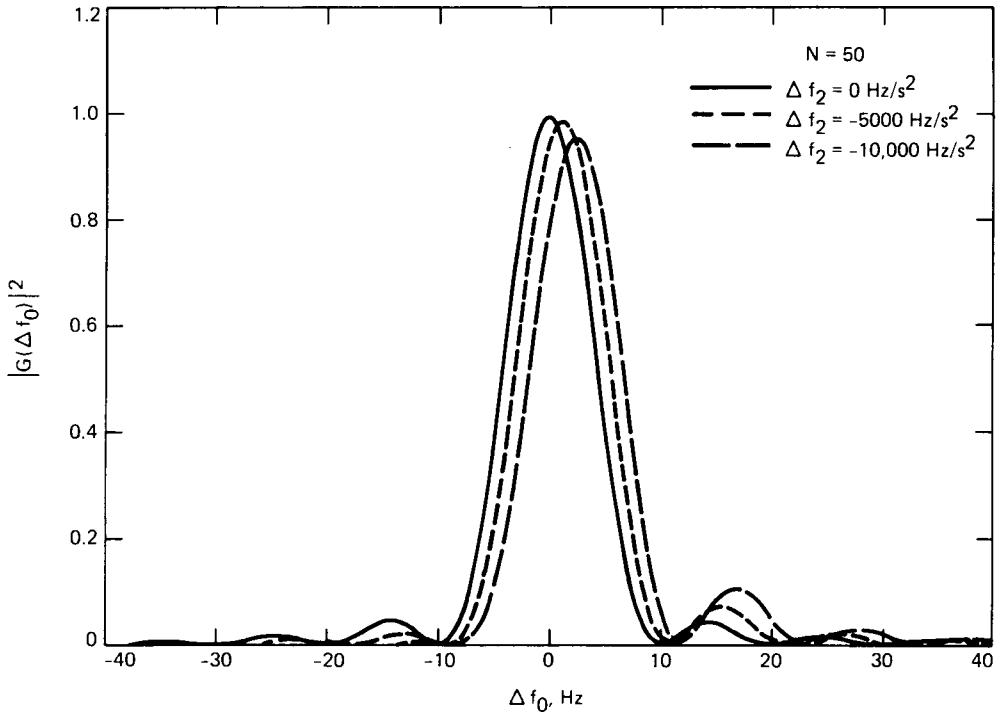

Figure 2(e). The Effect of Jerk Error on $|G(\Delta f_0)|^2$

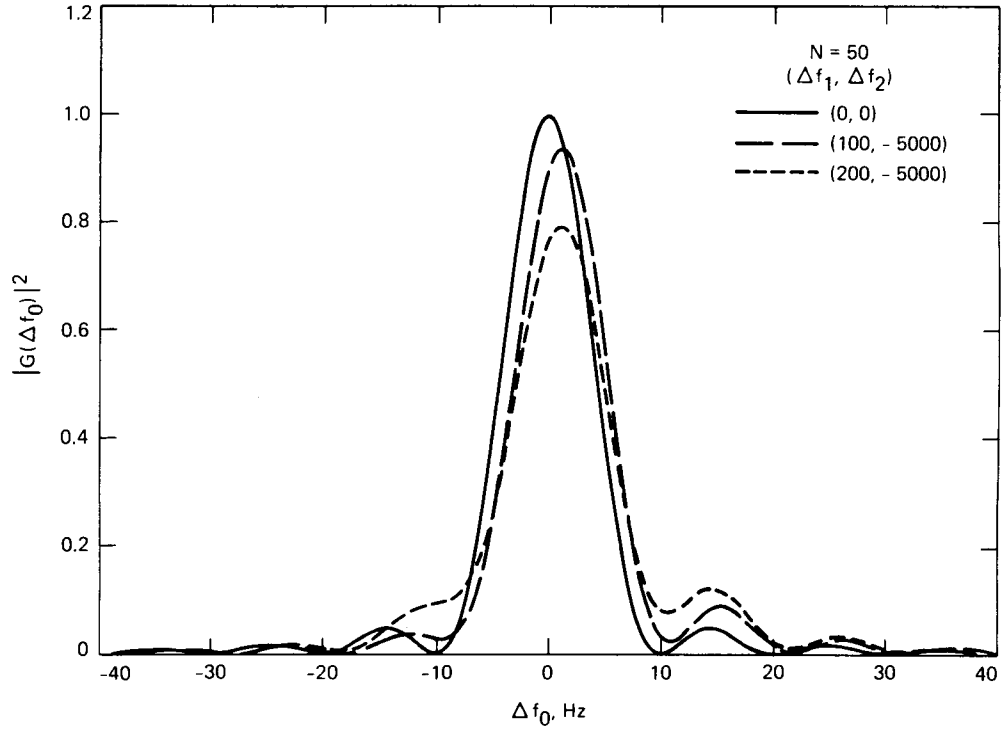

Figure 2(f). The Effect of Both Acceleration and Jerk Error on $|G(\Delta f_0)|^2$

The addition of noise impairs the estimator's ability to resolve the coordinates of the peak. The effects of additive noise can be quantified by means of the noise coherence function. For the case under consideration, we denote the effective three-dimensional transformed noise process by $n_3(f_0, f_1, f_2)$. Letting the signal component approach zero in Eq. (18), and using Eqs. (7) and (19), we obtain

$$E\{n_3(\underline{f} + \underline{\Delta f})n_3^*(\underline{f})\} = \sum_i \sum_\ell \overline{\tilde{n}_i \tilde{n}_\ell^*}\, e^{-j[g_i(\underline{f}+\underline{\Delta f})-g_\ell(\underline{f})]} \tag{20}$$

$$= N\left(\frac{N_0}{T_s}\right) G(\underline{\Delta f})$$

where

$$n_3(\underline{f}) \triangleq \sum_i \tilde{n}_i\, e^{-jg_i(\underline{f})}$$

Thus, Eq. (20) exhibits the same dependence on $\underline{\Delta f}$ as the function $G(\underline{\Delta f})$ defined in Eq. (19).

An analytic expression for the projection of $G(\underline{\Delta f})$ along the frequency coordinate follows by letting $t_i = (i + (1/2))\, T_s$ in Eq. (19):

$$G(\Delta f_0) = N^{-1} \frac{\sin(\pi \Delta f_0 N T_s)}{\sin(\pi \Delta f_0 T_s)} \tag{21}$$

This is recognized as the Fourier transform of an NT_s second pulse-train. However, for projections along the other coordinates, no closed form expressions could be found.

The Cramer-Rao bound for estimating the frequency of a pure tone without phase information is well known. Using the results of [2], and converting to our notation, we have

$$\mathrm{var}(\Delta\hat{f}_0) \geq \left(\frac{3}{2\pi^2}\right)\left(\frac{N_0}{A^2}\right)\frac{1}{T_s^3 N(N^2-1)} \quad ; \; N \geq 2, \text{ known frequency rate} \tag{22}$$

This bound applies to unbiased estimators. The variance of estimation error is inversely proportional to CNR, and for large N, inversely proportional to the cube of the total observation time. If the frequency drifts with some acceleration, then Eq. (22) may still apply at high CNR, provided the acceleration does not change significantly from one observation interval to the next, and assuming that it has been estimated accurately in the past. If, however, the acceleration changes significantly over the timescale of an observation interval, so that it cannot be assumed known, then Eq. (22) does not apply. In that case, the Cramer-Rao bound for estimating frequency in the presence of an unknown frequency rate should be used. This bound, derived in the Appendix, has the form

$$\mathrm{var}(\Delta\hat{f}_0) \geq 16\left(\frac{3}{2\pi^2}\right)\left(\frac{N_0}{A^2}\right)\frac{1}{T_s^3 N^3} \quad ; \; N \geq 2, \text{ unknown frequency rate} \tag{23}$$

for large N.

At low CNRs, estimator performance is critically linked to the total number of "coherence cells" in the observation volume. Referring to Figs. 2(a-c), the "coherence-length" δf_ℓ along the ℓth coordinate is defined as the distance from the peak to the first minimum of the function $|G(\underline{\Delta f})|^2$ along that coordinate. We immediately conclude from Eq. (21) that $\delta f_0 = 1/T_s N$. The values of δf_1 and δf_2 can be computed accurately for any value of N. Thus we may think of associating a distinct random variable with each coherence cell, statistically independent of all others.

Although the statistical distribution of the signal parameters is not known, we assume that with high probability their true value is contained in some "uncertainty volume" whose center and dimensions can be specified. This uncertainty volume may be thought of as a region in R_3 with dimensions (F_0, F_1, F_2), such that with high probability

$$-\frac{F_\ell}{2} \leq f'_\ell \leq \frac{F_\ell}{2}$$

for each ℓ. We shall show that the estimator threshold tends to decrease with decreasing volume, provided the true parameters remain within this volume.

The total number of independent random variables contained in an observation volume $V = F_0F_1F_2$ is

$$M = \left(\frac{F_0}{\delta f_0} + 1\right)\left(\frac{F_1}{\delta f_1} + 1\right)\left(\frac{F_2}{\delta f_2} + 1\right) \tag{24}$$

Thus we may think of partitioning the observation volume into M disjoint coherence cells, one of which contains signal plus noise, while the remaining (M-1) contain only noise. The noise samples associated with different coherence cells are independent complex Gaussian random variables, each with zero mean and variance $\sigma^2 = N(N_0/T_s)$. The mean value due to the signal is AN. The probability density of the magnitude of signal plus noise is the Rician density function

$$p_1(x) = \frac{2x}{\sigma^2} \exp\left(-\frac{(AN)^2 + x^2}{\sigma^2}\right) I_0\left(\frac{2ANx}{\sigma^2}\right) \tag{25}$$

while the noise sample magnitudes are distributed according to the Rayleigh density as

$$p_2(x) = \lim_{A \to 0} p_1(x) = \frac{2x}{\sigma^2} \exp\left(-x^2/\sigma^2\right) \tag{26}$$

In Eq. (25), $I_0(\cdot)$ denotes the modified Bessel function of zero order. Since the maximum likelihood estimator selects the coordinates of the largest peak as its estimate, large errors can occur if the magnitude of a noise sample in one or more coherence cells exceeds the magnitude of signal plus noise. This event is called an "outlier." Outliers occur with probability $q = 1 - p$, where

$$p = \int_0^\infty p_1(x) \left[\int_0^x p_2(y)\, dy \right]^{M-1} dx \tag{27}$$

Note that p and q depend only on the ratio $(NA)^2/\sigma^2 = A^2 T_s / N_0$ and M. The behavior of q as a function of CNR is shown in Fig. 3 for NT_s = 100 msec and various M. It is apparent that for 100 msec observation times the probability of selecting the wrong observation volume is small for CNRs greater than 23 dB-Hz, while at lower CNRs outliers are virtually certain. At any CNR, q is an increasing function of M, hence it is advantageous to keep M small in order to avoid frequent outliers, leading to large estimation errors.

Given that an outlier occurred, the estimation error variance can be found by assuming that each point within the observation region has equal a priori

probability of being chosen, hence the frequency estimate may take on any value between $-F_0/2$ and $F_0/2$. Therefore,

$$\text{var}(\Delta\hat{f}_0|\text{cell error}) = F_0^{-1} \int_{-F_0/2}^{F_0/2} x^2\, dx = \frac{F_0^2}{12} \qquad (\text{Hz}^2) \tag{28}$$

The high CNR result of Eq. (22) may be interpreted as the variance of the estimation error given that the correct coherence-cell was chosen, that is,

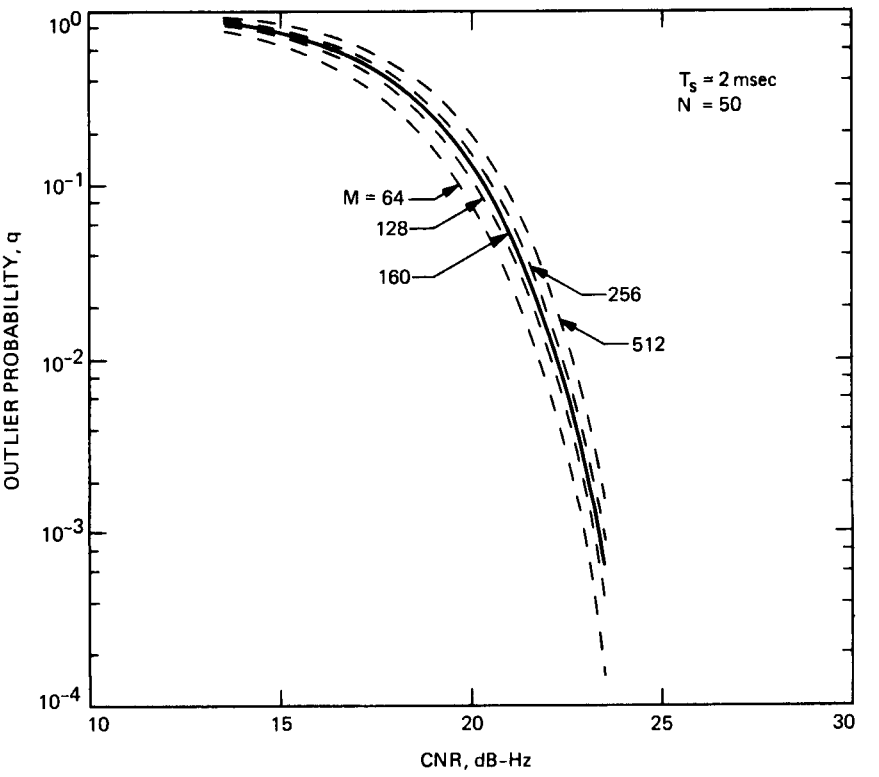

Figure 3. Outlier Probability q as a Function of CNR

$\text{var}(\Delta\hat{f}_0|\text{no cell error})$. At any CNR, the variance of frequency estimation error is given by

$$\text{var}(\Delta\hat{f}_0) = q\ \text{var}(\hat{f}_0|\text{cell error}) + p\ \text{var}(\hat{f}_0|\text{no cell error}) \tag{29a}$$

which can be bounded in terms of the underlying parameters as

$$\text{var}(\Delta\hat{f}_0) \geq q\left(\frac{F_0^2}{12}\right) + p\left[\left(\frac{3}{2\pi^2}\right)\left(\frac{N_0}{A^2}\right)\left(\frac{1}{T_s^3 N(N^2-1)}\right)\right] \tag{29b}$$

The standard deviation of the estimation error as a function of CNR is shown in Fig. 4, for N = 50, T_s = 2 msec and M = 160. For this example, the boundary between the high and low CNR regions is roughly 24 dB-Hz. This boundary need not correspond exactly to the loss-of-lock threshold, which we define as the CNR at which the estimator loses lock ten percent of the time.

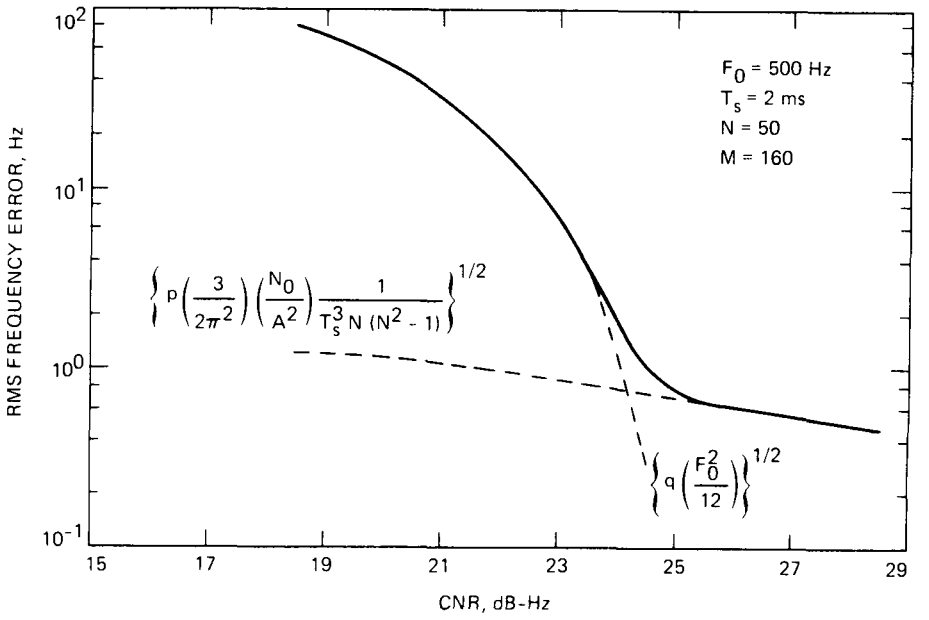

Figure 4. RMS Frequency Error and its Components (ML)

c. Simulation Results.

Estimator performance was verified by means of numerical simulations. The received samples were obtained from the common trajectory by sampling at 2-msec intervals, generating complex signal samples with the proper phase variation, and adding independent complex noise samples. In this implementation, N consecutive samples were processed by the estimator at one time, and the resulting parameter estimates referred to the center of the observation interval. These current estimates were used to predict the center of the observation volume for the following interval.

A discrete approximation to the maximum likelihood estimator may be obtained by evaluating $L(\underline{f})$ at uniformly spaced points along each coordinate of the uncertainty volume, with spacing fine enough to resolve the main lobe. Using this approach, efficient fast-Fourier transform (FFT) techniques may be employed to reduce the computational burden. In the current application, the simulated trajectory is dominated by 100-g/sec pulses of 0.5-sec duration. Since the sampling rate is fixed, the maximum change in acceleration increases with the total number of consecutive samples N. However, during constant acceleration, the rms estimation error decreases with increasing N. Thus we expect that for a given set of dynamic conditions an optimum value of N exists that provides high CNR without incurring excessive change in acceleration, which would require extending the acceleration uncertainty interval.

The dimensions of the uncertainty volume and the number of discrete grid points along each coordinate are fundamental simulation parameters. Referring to Fig. 2(c) we note that for N = 50 and T_s = 2 msec, the main lobe along the

Δf_2 coordinate extends to about ± 40000 Hz/sec^2. We also observe from Fig. 2(e) that an error in jerk of ± 100 g/sec $\cong \pm 5000$ Hz/sec^2 causes only a slight decrease in the peak of $|G(\Delta f_0)|^2$ and a relatively small shift in frequency. Since we are primarily interested in estimator performance near threshold where frequency errors tend to be large, it seems reasonable to ignore the variation in jerk, and effectively assume it to be zero throughout the trajectory. Of course, this approximation impacts estimator performance at CNRs well above threshold, where the dominant source of frequency error now becomes the shift in the peak due to the non-zero jerk.

Since we are projecting the estimates ahead in time to the center of the following observation interval, the maximum change in acceleration that can occur in $NT_s = 100$ msec due to ± 100-g/sec jerk is ± 10 g $\cong \pm 500$ Hz/sec. Thus we let $(F_1/2) \geq 10$ g, and partition F_1 into 2.5-g increments covering a range of ± 15 g, including a margin. The resulting 13-point grid samples $G(\Delta f_1)$ at 125-Hz/sec intervals, easily resolving the main lobe.

Finally, we recall that $F_0 = 1/T_s = 500$ Hz. Since the first zero along the frequency coordinate occurs at 10 Hz, the main lobe is well resolved by oversampling at roughly 2 Hz, implying the use of a 256-point FFT (the power of two nearest 250). Thus, we append 206 zeros to the 50 samples, and perform 256-point FFTs for each of 13 acceleration increments. From Eq. (24), using the value $\delta f_1 \cong 700$ Hz, the total number of independent random variables in this observation volume is $M = [(500/10) + 1][(1500/700) + 1] \cong 160$, which is the value used in the computation of the outlier probabilities.

Representative sample sequences of frequency and frequency rate estimation errors are shown in Figs. 5(a) and 5(b), at a CNR of 23 dB-Hz. Note the highly quantized nature of the frequency rate estimation error, due to the 2.5-g quantization of the acceleration estimate. At such low carrier-to-noise ratios the estimator sometimes loses lock before completing the entire trajectory.

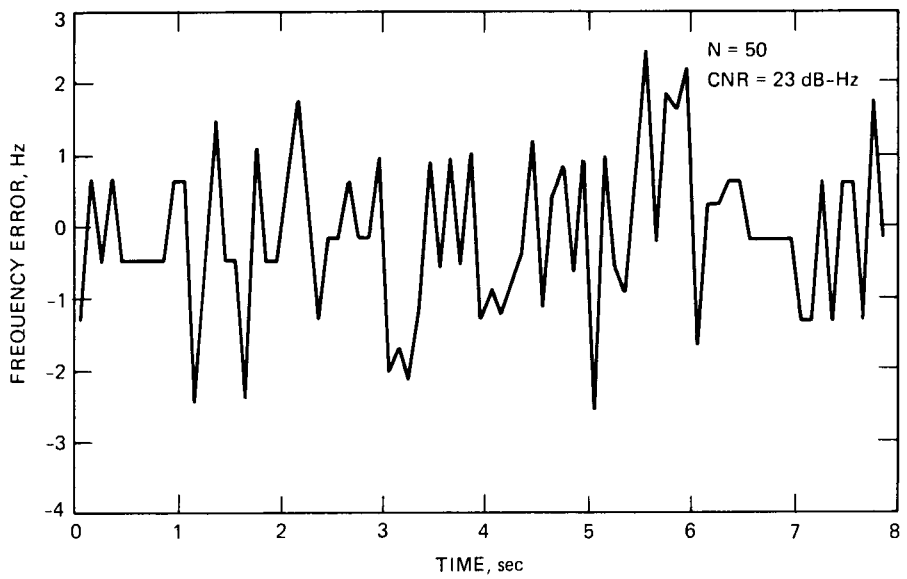

Figure 5(a). Instantaneous Frequency Error as a Function of Time (ML)

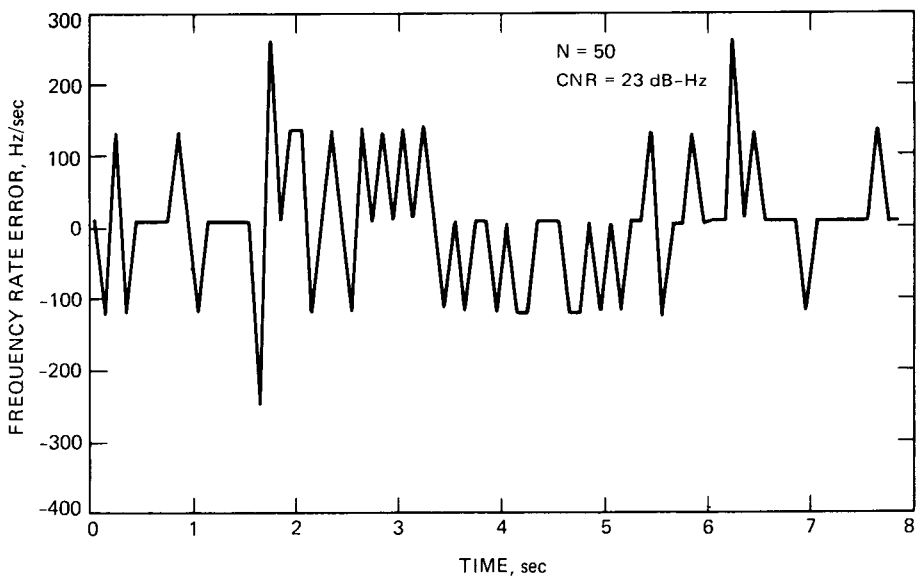

Figure 5(b). Instantaneous Frequency Rate Error as a Function of Time (ML)

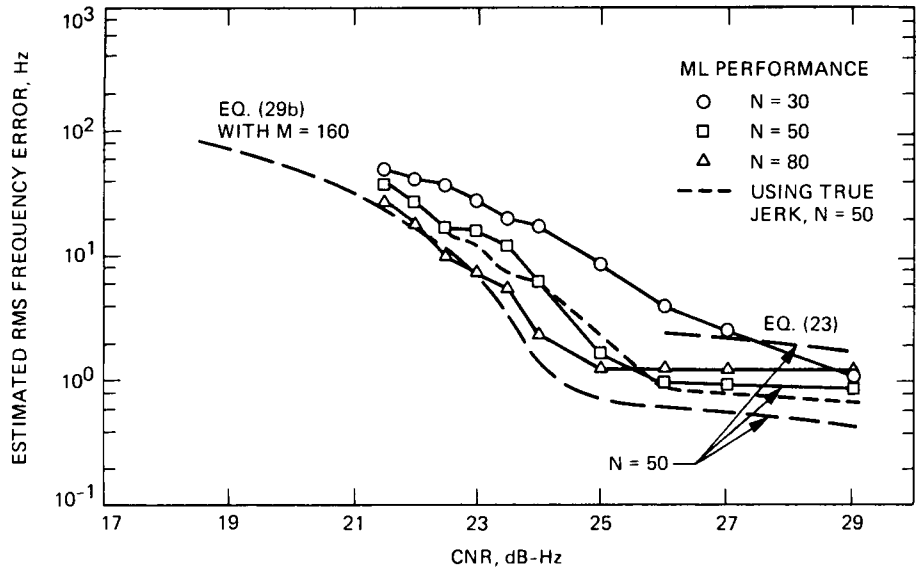

Figure 6(a). Estimated RMS Frequency Errors as Functions of CNR (ML)

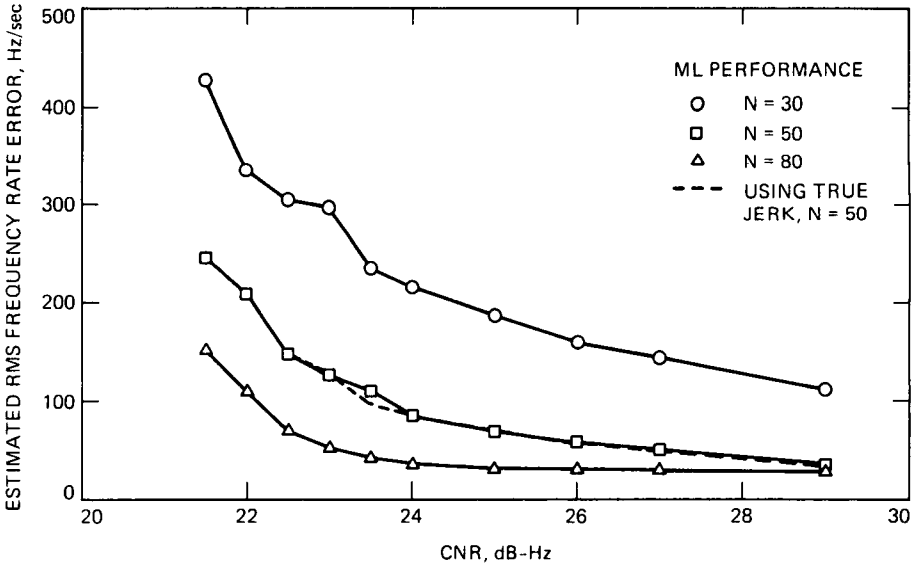

Figure 6(b). Estimated RMS Frequency Rate Errors as Functions of CNR (ML)

Estimates of the rms frequency estimation errors are shown in Fig. 6(a) for N = 30, 50, and 80 using 2-g, 2.5-g, and 3-g acceleration quantization, respectively. The saturation in the estimation error at CNRs above 26 dB-Hz for N = 50 and 80 is attributed to the shift in the peak of the likelihood function introduced by the non-zero jerk pulses. These errors tend to increase with N because the magnitude of the shift is proportional to the observation interval. Simulation results for N = 50 were also obtained using

the true value of the jerk in order to bound the improvement in the frequency estimates that could be obtained if the jerk were estimated as well. The dotted curve in Fig. 6(a) presents the results. Apparently, no improvement is possible at or below threshold. Above threshold, however, frequency estimation errors could be reduced by the simultaneous estimation of jerk, acceleration, and velocity components. From Fig. 6(b) we note that the frequency rate estimates are not affected by mismodeling the jerk, at least in the range of the CNRs considered.

If the predicted frequency for the upcoming observation volume is in error by more than $\pm$250 Hz, then the signal parameters most likely fall outside the succeeding observation volume, in which case loss-of-lock occurs. The loss-of-lock probability p is approximated by counting the number of times the estimator loses lock in 100 independent simulations. Estimates of the loss-of-lock probability are shown in Fig. 7 for N = 30, 50, and 80 samples per estimate. Note that loss-of-lock probabilities do not improve significantly if the true jerk is used, as shown by the dotted curve.

Finally we observe that estimator performance could be improved somewhat by searching over a subset of the uncertainty volume. This approach is motivated by the observation that the maximum change in frequency is limited to $\pm$125 Hz, due to 25-g acceleration applied for 0.1 sec. Hence the total number of degrees of freedom becomes $M \cong 26 \times 3 = 78$, which may result in a 0.3-dB reduction in the threshold. However, such fine-tuning is possible only because the trajectory parameters are well known. If that were not the case, this minor improvement may well be cancelled by the increased design margin required to compensate for the greater initial uncertainties.

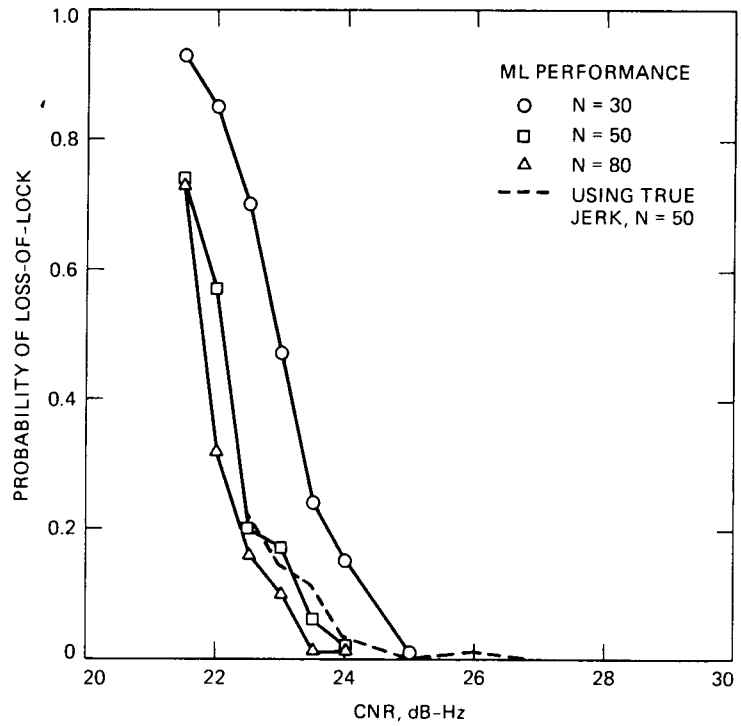

Figure 7. Estimated Loss-of-Lock Probabilities as Functions of CNR (ML)

EXTENDED KALMAN FILTER (EKF)

Here we consider the application of an extended Kalman filter (EKF) to the problem of estimating the parameters of the received signal, driven by the common trajectory. A fundamental difference between this and the maximum likelihood approach is that the EKF provides instantaneous estimates after each new sample based on the latest sample value and previous estimates, whereas the maximum likelihood estimator provides estimates of average parameter values after processing a large number of samples. We begin by deriving the structure of the EKF estimator.

a. Extended Kalman Filter Estimator Structure.

In this derivation we adopt vector notation, both for convenience and to conform to established practice. The received samples defined in Eq. (6) are now expressed as

$$\underline{r}(k) = \begin{bmatrix} A \sin [\theta(k)] \\ \\ A \cos [\theta(k)] \end{bmatrix} + \underline{n}(k) \tag{30}$$

where $\underline{n}^T(k) = [n_I(k), n_Q(k)]$ is a zero-mean Gaussian vector, with the subscripts I and Q denoting in-phase and quadrature components, respectively. These correspond to the real and imaginary components of the complex noise sample defined in Eq. (6). From here on, the amplitude A is set to unity as it is assumed known and need not be estimated by the EKF. As before, we have

$$E[\underline{n}(k)] = \underline{0} \tag{31a}$$

$$E[\underline{n}(k)\ \underline{n}^T(\ell)] = \begin{cases} \underline{0} & k \neq \ell \\ \sigma_n^2 \underline{\underline{I}} & k = \ell \end{cases} \tag{31b}$$

with I denoting the 2 x 2 identity matrix, and $\sigma_n^2 = N_0/2T_s$. The extended Kalman filter operates on the phase $\theta(k)$ which is a sampled version of the integral of the frequency trajectory. The phase can be modeled as an n-th order polynomial whose derivatives constitute the components of the state-vector $\underline{x}(k)$ as follows:

$$\theta(k) = \underline{\ell}^T \underline{x}(k) \ ; \quad \underline{\ell}^T = [1, 0, \ldots, 0] \tag{32a}$$

$$\underline{x}(k + 1) = \underline{\underline{\Phi}}\ \underline{x}(k) + \underline{\nu}(k) \tag{32b}$$

In the above, $\underline{\underline{\Phi}}$ denotes the state transition matrix and $\underline{\nu}(k)$ is the disturbance vector. For a fourth-order EKF, $\underline{x}^T(k)$ becomes

$$\underline{x}^T(k) = [\theta(k), \omega_0(k), \omega_1(k), \omega_2(k)] \tag{33}$$

where the various derivatives of $\theta(k)$ are denoted by $\omega_0(k)$, $\omega_1(k)$, and $\omega_2(k)$, respectively. Here each ω_ℓ is 2π times as great as the corresponding f_ℓ defined previously. The disturbance term models the random changes in the parameters due to dynamics. Since consecutive components of the state vector are integrals of the succeeding ones, repeated integration over the observation time yields

$$\omega_2(k+1) = \omega_2(k) + \nu_4(k) \tag{34a}$$

$$\omega_1(k+1) = \omega_1(k) + T_s\omega_2(k) + \nu_3(k) \tag{34b}$$

$$\omega_0(k+1) = \omega_0(k) + T_s\omega_1(k) + \frac{T_s^2}{2}\omega_2(k) + \nu_2(k) \tag{34c}$$

$$\theta(k+1) = \theta(k) + T_s\omega_0(k) + \frac{T_s^2}{2}\omega_1(k) + \frac{T_s^3}{6}\omega_2(k) + \nu_1(k) \tag{34d}$$

where

$$\nu_i(k) = \int_{(k-1)T_s}^{kT_s} \frac{\tau^{4-i}}{(4-i)!}\, Y(\tau)\, d\tau \;; \quad i = 1, \ldots, 4 \tag{35}$$

and Y(t) denotes the fourth derivative of the continuous version of the phase. Assuming that Y(t) is a zero-mean white process with spectral level N_y, we get

$$E[\nu_4^2(k)] = \frac{N_y}{2} T_s = \sigma_y^2 T_s^2 \tag{36}$$

with σ_y^2 denoting the variance of the sampled version of Y(t), and N_y the level of the power spectral density of Y(t). The system matrix $\underline{\underline{\Phi}}$ and the covariance matrix $\underline{\underline{Q}}$ of the disturbance vector $\underline{\nu}(k)$ can be derived from Eqs. (34) and (35), as in [3]:

$$\underline{\underline{\Phi}} = \begin{bmatrix} 1 & T_s & T_s^2/2 & T_s^3/6 \\ 0 & 1 & T_s & T_s^2/2 \\ 0 & 0 & 1 & T_s \\ 0 & 0 & 0 & 1 \end{bmatrix} \tag{37a}$$

$$\underline{\underline{Q}} = N_y T_s \begin{bmatrix} T_s^6/252 & T_s^5/72 & T_s^4/30 & T_s^3/24 \\ T_s^5/72 & T_s^4/20 & T_s^3/8 & T_s^2/6 \\ T_s^4/30 & T_s^3/8 & T_s^2/3 & T_s/2 \\ T_s^3/24 & T_s^2/6 & T_s/2 & 1 \end{bmatrix} \tag{37b}$$

The following equations can then be derived for the estimation of the state vector $\underline{x}(k)$, as in [4]:

$$\hat{\underline{x}}(k|k) = \hat{\underline{x}}(k|k-1) + \underline{\underline{L}}(k)[\underline{r}(k) - \underline{h}(\hat{\underline{x}}(k|k-1))] \tag{38a}$$

$$\hat{\underline{x}}(k+1|k) = \underline{\underline{\Phi}}\, \hat{\underline{x}}(k|k) \tag{38b}$$

$$\underline{\underline{\Omega}}(k) = H^T(k)\, \underline{\underline{P}}(k|k-1)\, \underline{\underline{H}}(k) + \underline{\underline{R}} \tag{38c}$$

$$\underline{\underline{L}}(k) = \underline{\underline{P}}(k|k-1)\, \underline{\underline{H}}(k)\, \underline{\underline{\Omega}}^{-1}(k) \tag{38d}$$

$$\underline{\underline{P}}(k|k) = \underline{\underline{P}}(k|k-1) - \underline{\underline{P}}(k|k-1)\, \underline{\underline{H}}(k) \times (\underline{\underline{H}}^T(k)\, \underline{\underline{P}}(k|k-1)\, \underline{\underline{H}}(k) + \underline{\underline{R}})^{-1}\, \underline{\underline{H}}^T(k)\, \underline{\underline{P}}(k|k-1) \tag{38e}$$

$$\underline{\underline{P}}(k+1|k) = \alpha^2\, \underline{\underline{\Phi}}\, \underline{\underline{P}}(k|k)\, \underline{\underline{\Phi}}^T + \underline{\underline{Q}} \tag{38f}$$

where $\underline{\underline{R}} = \sigma_n^2\, \underline{\underline{I}}$, α is some weighting coefficient greater than one, and $\underline{\underline{H}}^T(k)$ is the linearization of the function $\underline{h}(\underline{x}(k))$, i.e.,

$$\underline{\underline{H}}^T(k) = \frac{\partial}{\partial x}\, \underline{h}(\underline{x})\Big|_{\underline{x} = \hat{\underline{x}}(k|k-1)} \tag{39}$$

where

$$\underline{h}(\underline{x}|\underline{k}) = \begin{bmatrix} \sin(\underline{\ell}^T\, \underline{x}(k)) \\ \\ \cos(\underline{\ell}^T\, \underline{x}(k)) \end{bmatrix}$$

The constant α is used to adjust the weighting of past data in order to speed up filter response in transient situations.

b. Estimator Performance.

The performance of the fourth-order extended Kalman filter operating in dynamic environments and in the presence of additive noise can be bounded by means of the Cramer-Rao bounds. At high CNRs and mild dynamics the Cramer-Rao bound of Eq. (22) should apply, since this filter is an approximation to an optimum tracking algorithm. For high dynamics, where the variation in acceleration is significant, the bound for unknown acceleration, Eq. (23), should apply. Since this bound requires knowledge of the effective integration time, this quantity has to be determined. Response to dynamics, however, will only be assessed by means of the simulation results, except to note that dynamics tends to move the performance curves closer to the bound for unknown acceleration.

c. Simulation Results.

The performance of the EKF while tracking the common simulated trajectory has been evaluated. Both third- and fourth-order filters were considered. Since our primary interest is in evaluating tracking ability rather than acquisition, we assume that the initial conditions of the trajectory are precisely known. Thus the state components of the EKF are initially matched to the true trajectory. The exponential weighting coefficient α controls the memory of the filter. To reduce the effects of additive noise, α should be set to one in order to average over all previous data. In a dynamic

environment α is adjusted such that the present estimate is dominated by the past $1/(\alpha - 1)$ data points. For fixed sampling times, this establishes the equivalent integration time to be used in the Cramer-Rao bounds. An exponential weighting coefficient of 1.027 was used for the fourth-order EKF, as this value yielded the best performance. This corresponds to an effective memory of roughly 40 samples.

A typical sample sequence of the instantaneous phase error is shown in Fig. 8(a) at a CNR of 26 dB-Hz, using a fourth-order EKF. It can be seen that the trajectory has little effect on the instantaneous phase error, while the instantaneous frequency and frequency rate errors tend to peak near the beginning and the end of each jerk pulse (Figs. 8[b] and [c]). This occurs because the peaks due to the trajectory are exaggerated by the presence of noise due to nonlinear effects within the estimator. Estimates of the loss-of-lock probability for phase and frequency estimates are shown in Figs. 9(a) and (b) for third- and fourth-order EKFs. Defining the threshold to be the CNR that yields 10% probability of loss-of-lock, it is clear that the fourth-order filter has a phase threshold of about 24.5 dB-Hz and a frequency threshold of roughly 24 dB-Hz. The rms phase, frequency, and frequency rate errors as functions of CNR are shown in Figs. 10(a), (b), and (c). At threshold, the minimum rms phase error is 0.4 rad, the minimum rms frequency error is about 3 Hz, while the minimum rms frequency rate error is roughly 75 Hz/sec. Note that the filter configuration with the lowest threshold does not achieve the lowest rms estimation errors. This is because the filter parameters were selected for minimizing loss-of-lock threshold rather than estimation error.

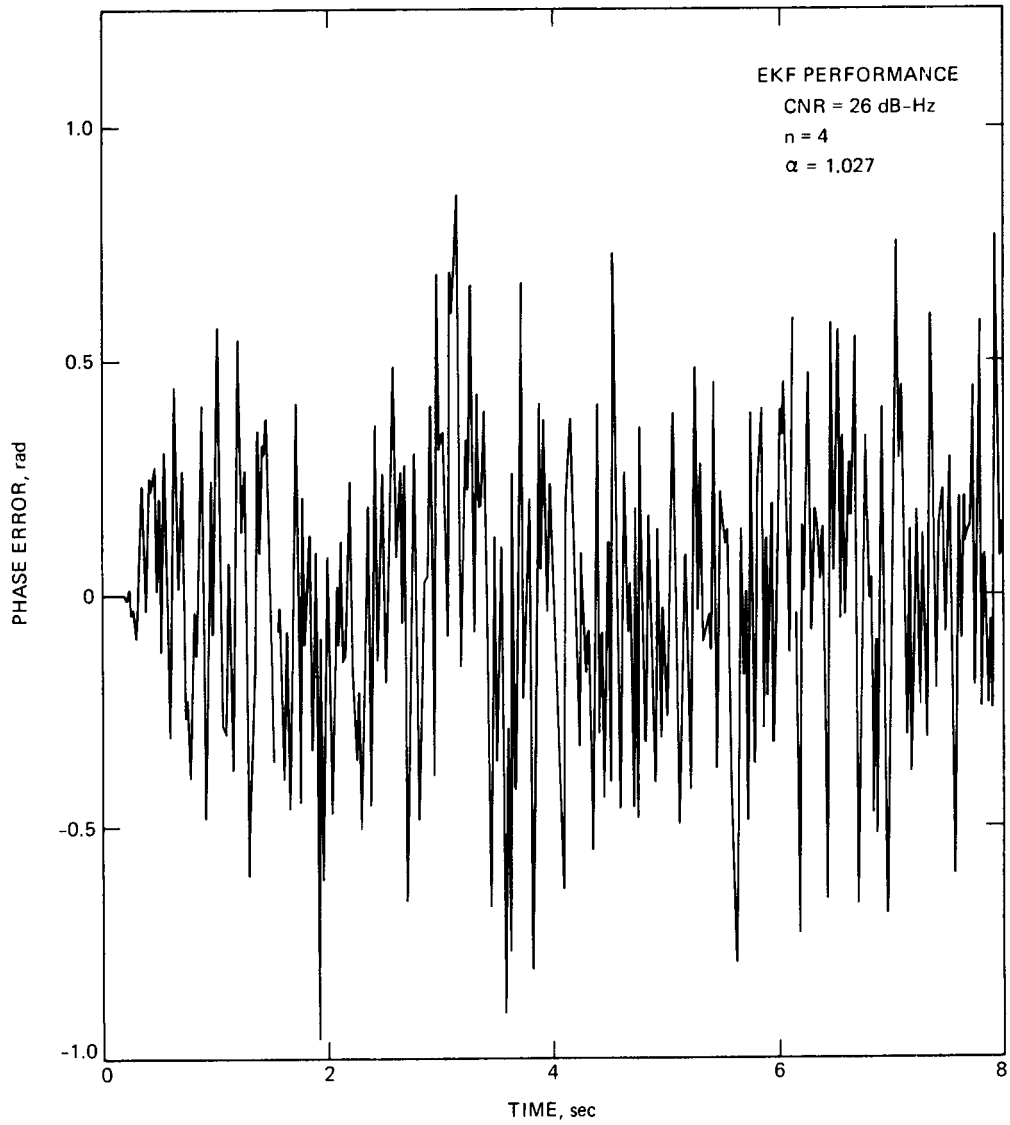

Figure 8(a). Instantaneous Phase Error as a Function of Time (EKF)

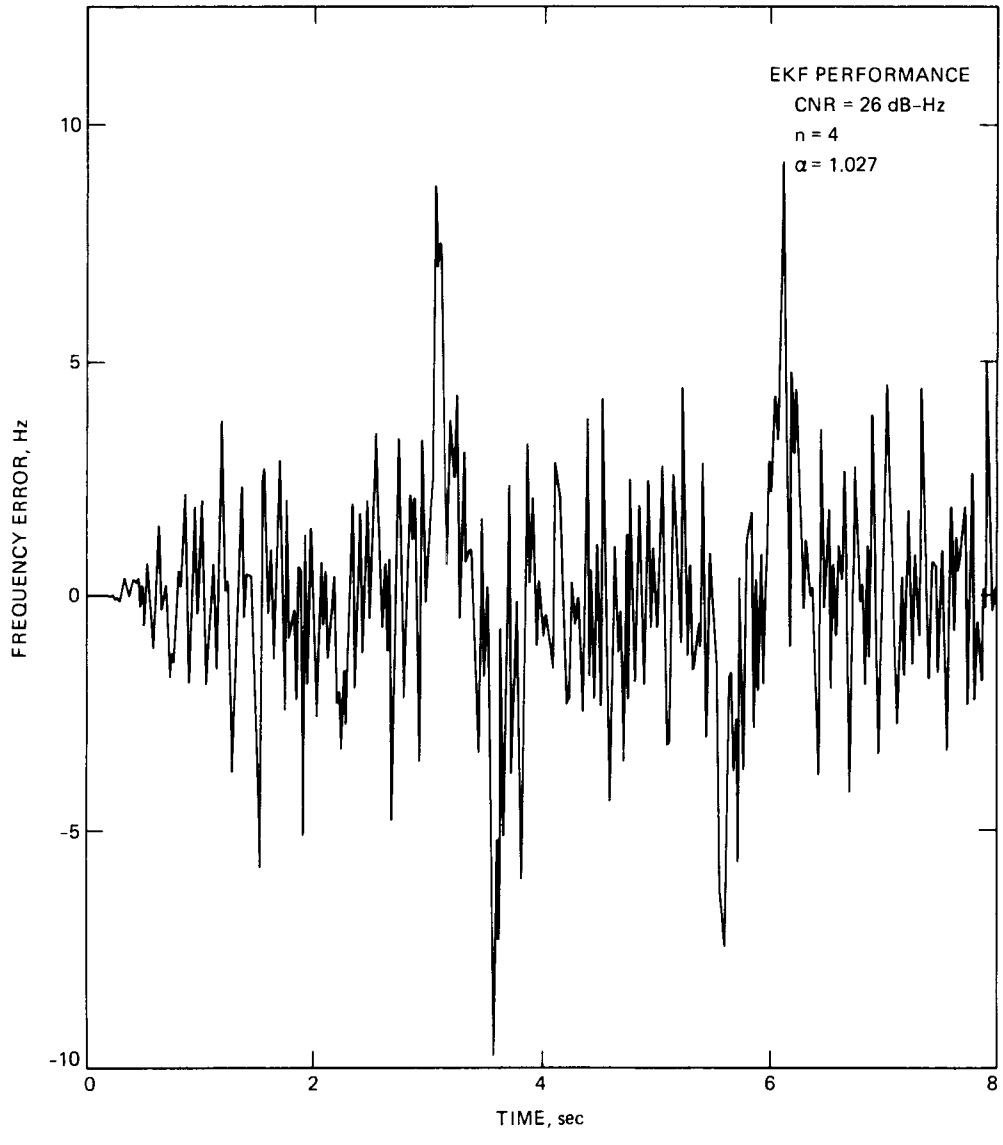

Figure 8(b). Instantaneous Frequency Error as a Function of Time (EKF)

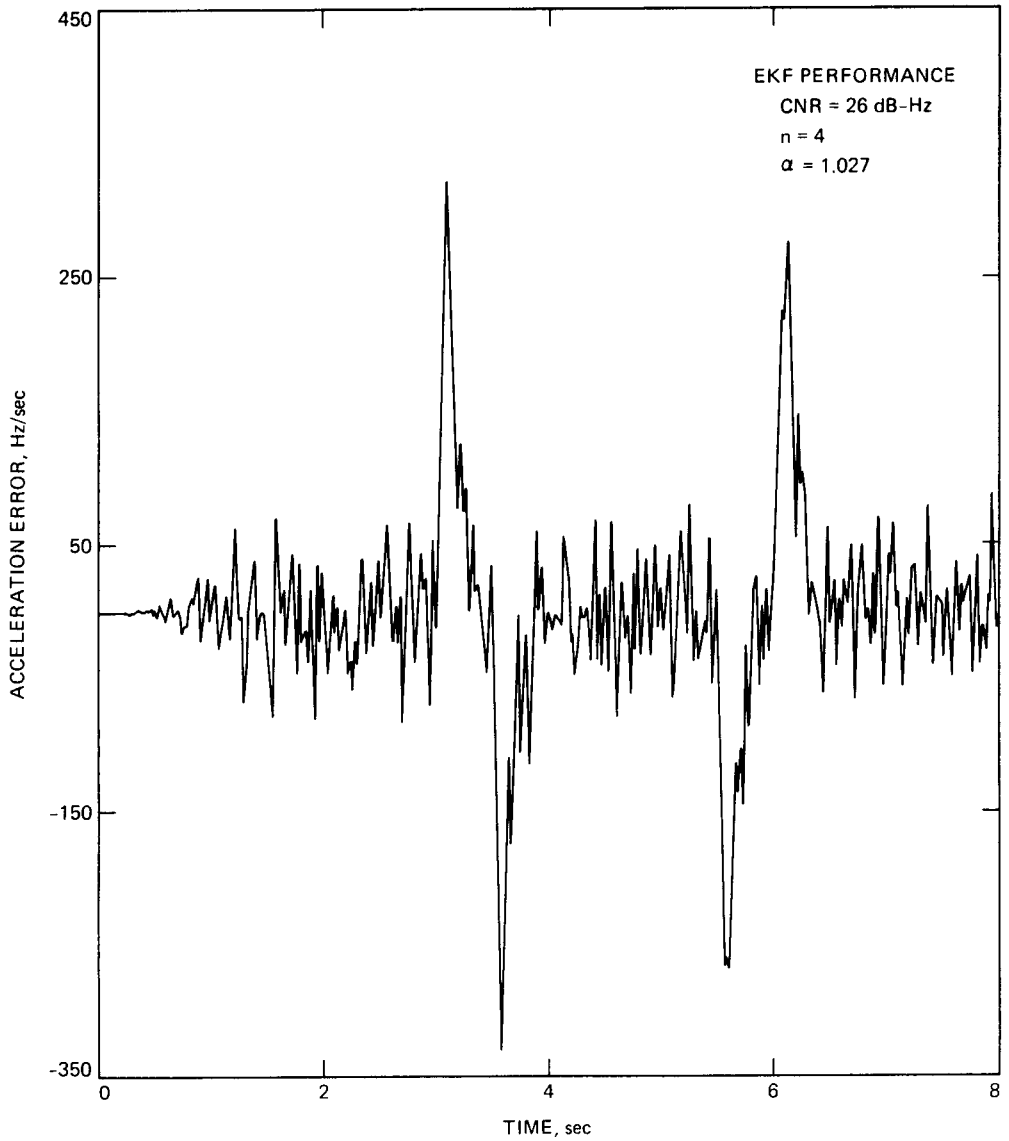

Figure 8(c). Instantaneous Acceleration Error as a Function of Time (EKF)

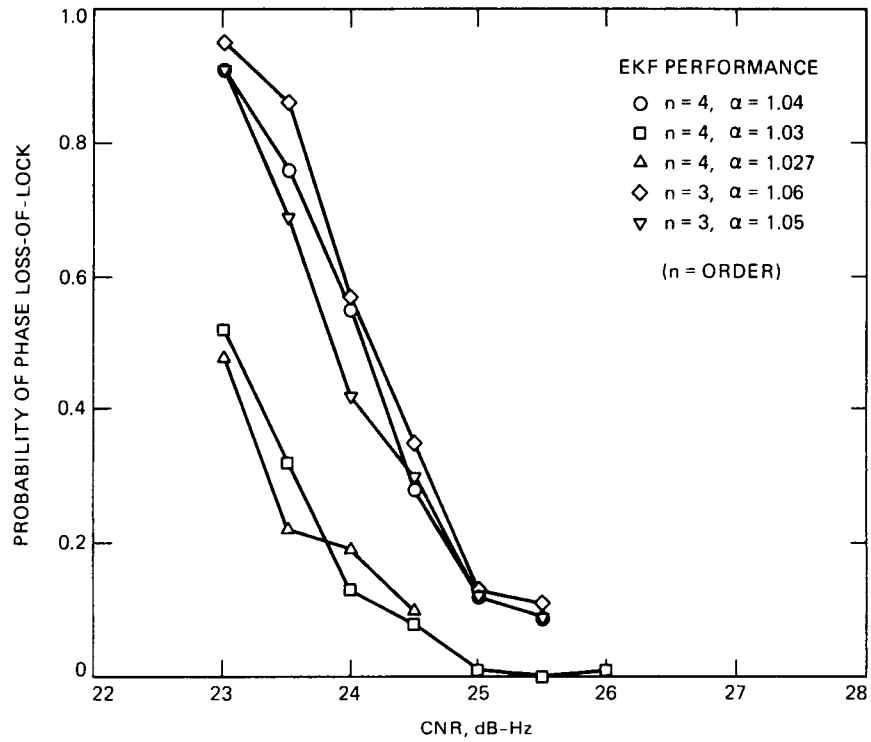

Figure 9(a). Estimated Phase Loss-of-Lock Probabilities as Functions of CNR (EKF)

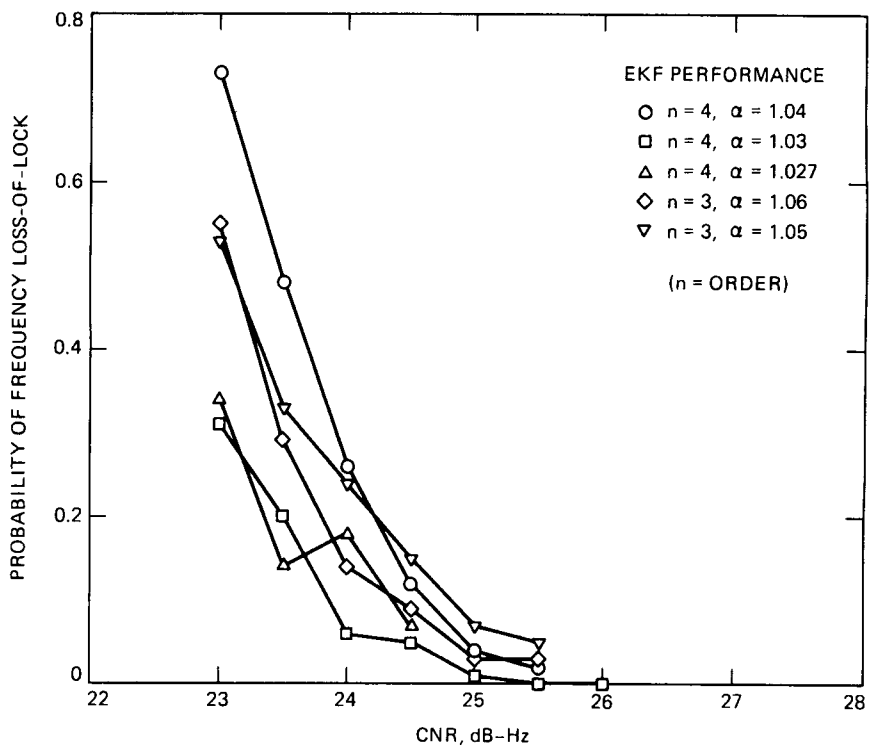

Figure 9(b). Estimated Frequency Loss-of-Lock Probabilities as Functions of CNR (EKF)

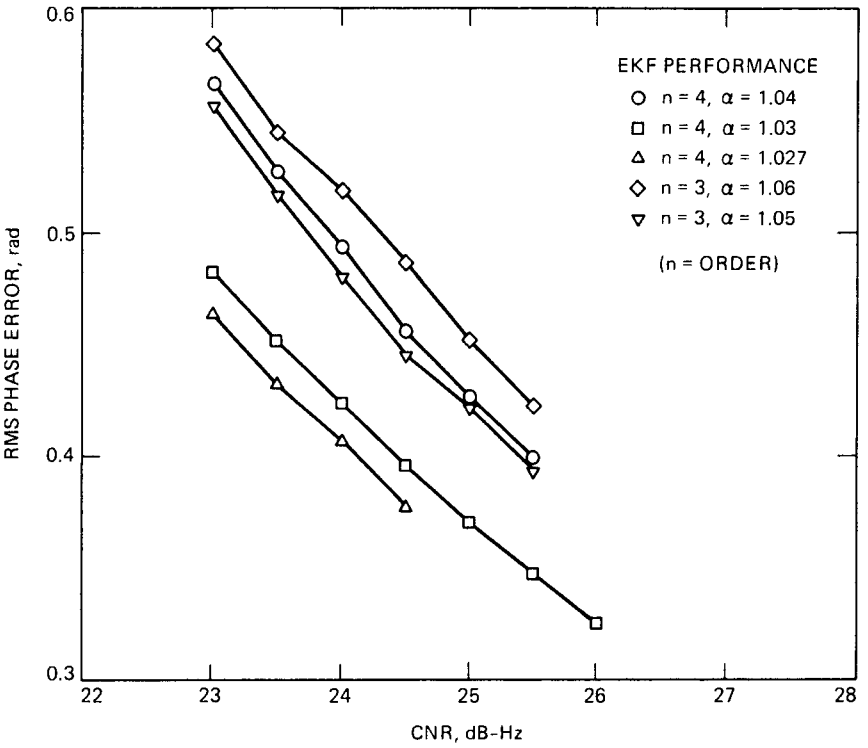

Figure 10(a). Estimated RMS Phase Errors as Functions of CNR (EKF)

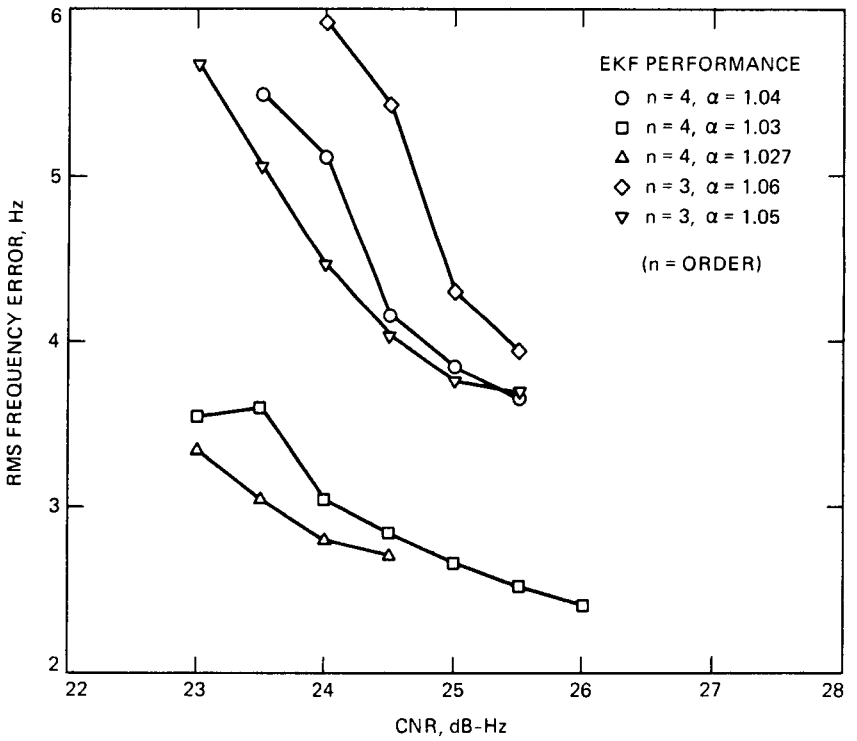

Figure 10(b). Estimated RMS Frequency Errors as Functions of CNR (EKF)

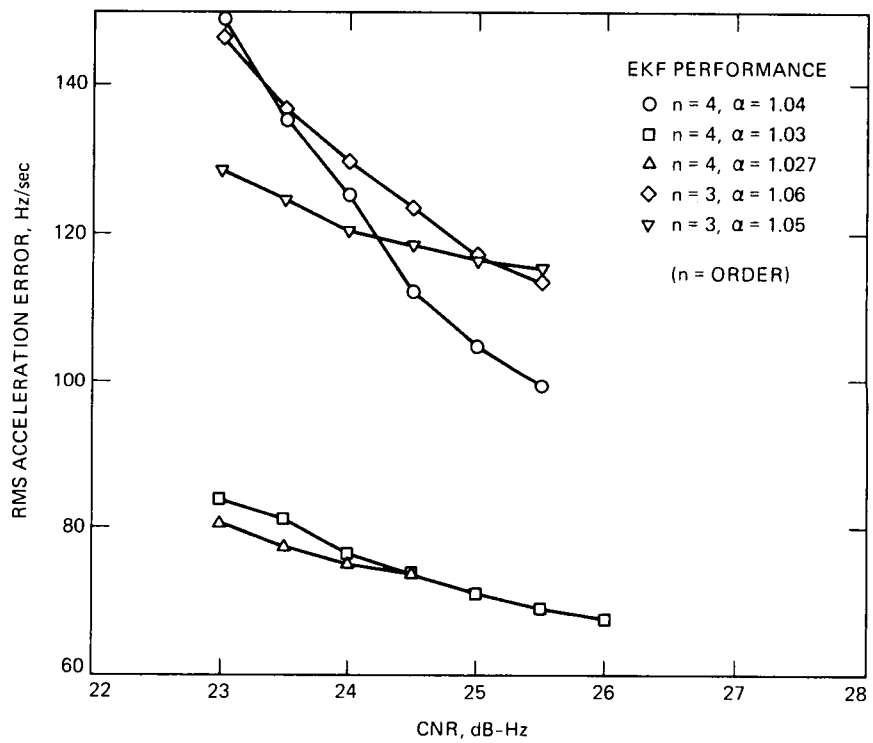

Figure 10(c). Estimated RMS Acceleration Errors as Functions of CNR (EKF)

CROSS-PRODUCT AUTOMATIC FREQUENCY CONTROL (CPAFC) LOOP

In this approach a frequency discriminator is employed to track the received frequency. An automatic frequency control (AFC) configuration that employs a cross-product discriminator is also referred to as a "quadri-correlator" AFC loop.

a. CPAFC Loop Estimator Structure.

The discriminator output is represented in [5] by

$$V_k = I_{k-1} Q_k - Q_{k-1} I_k \tag{40}$$

where I and Q are the outputs of the in-phase and quadrature mixers. The performance of this loop operating in the presence of additive white Gaussian noise has been analyzed in [5] for a general loop filter. In our application the loop filter was chosen to be of the form

$$F(z) = \frac{k_1}{1 - z^{-1}} + \frac{k_2}{(1 - z^{-1})^2} \tag{41}$$

where z is the independent variable of the z-transform, $k_1 = rd/T_s$, $k_2 = rd^2/T_s$, $d = 4B_L T_s/(r + 1)$, B_L is the nominal bandwidth of the cross-product AFC loop, r is the damping parameter, and T_s the loop update time. This loop is capable of tracking acceleration with zero steady-state frequency error.

b. Estimator Performance.

In the absence of jerk and higher-order derivatives in the trajectory, the loop defined above tracks frequency variations with zero error in the absence of additive noise. However, jerk introduces a steady-state error that cannot be overcome with this loop. The addition of noise also degrades estimator performance, increasing the estimation error variance inversely with the carrier-to-noise ratio. Thus it makes sense to examine performance degradation due to either dynamics or additive noise separately, while the contribution of the other component is ignored. This allows us to assess loop performance when either component dominates. In general, both components contribute to the total estimation error.

First we consider the steady-state frequency estimation error induced by a constant jerk of magnitude J. From [6], the steady-state frequency error due to constant jerk of magnitude J (m/sec^3) is

$$f_{ss} = 5.25 \frac{J}{r} \left(\frac{r + 1}{4B_L} \right)^2 \qquad (Hz) \tag{42}$$

which depends directly on the jerk, but inversely on the square of the nominal loop bandwidth. The variance of the frequency estimation error due to zero-mean additive Gaussian noise was found [6] to be

$$\sigma_f^2 = 0.051 \left(\frac{N_0}{A^2} \right) \frac{B_L}{T_s^2} \qquad (Hz^2) \tag{43}$$

The error variance is seen to be inversely proportional to CNR and the square of the update time, but increases linearly with loop bandwidth. Comparing Eq. (42) with Eq. (43), we see that increasing the loop bandwidth yields improved steady-state performance at the cost of degraded noise performance. Thus, conflicting requirements must be balanced when both additive noise and severe trajectory variations are present.

c. Simulation Results.

The performance of the cross-product AFC loop was evaluated by means of numerical simulations. For the trajectory under consideration, it was found that a nominal loop bandwidth of B_L = 8 Hz minimized the loss-of-lock threshold. At a carrier-to-noise ratio of 25 dB-Hz, with jerk of magnitude 100 g/sec, this bandwidth yields a calculated steady-state frequency error of f_{ss} = 22.6 Hz, and a noise-induced rms frequency error of roughly σ_f = 18 Hz. The simulations confirmed these predictions.

A typical frequency error trajectory is shown in Fig. 11 at a CNR of 26 dB-Hz. The average frequency error appears to remain constant throughout the trajectory. Fig. 12(a) shows the estimated loss-of-lock performance of the loop for various bandwidths and damping ratios, while Fig. 12(b) displays the corresponding rms frequency errors as a function of CNR. The lowest loss-of-lock threshold appears to be 24.5 dB-Hz, achieved by a 7-Hz loop with a damping ratio of 2. The corresponding rms frequency error is roughly 40 Hz for this case. We observe that small variations in bandwidth do not affect the loss-of-lock performance of the AFC loop significantly, but seem to have a more serious effect on the rms estimation error.

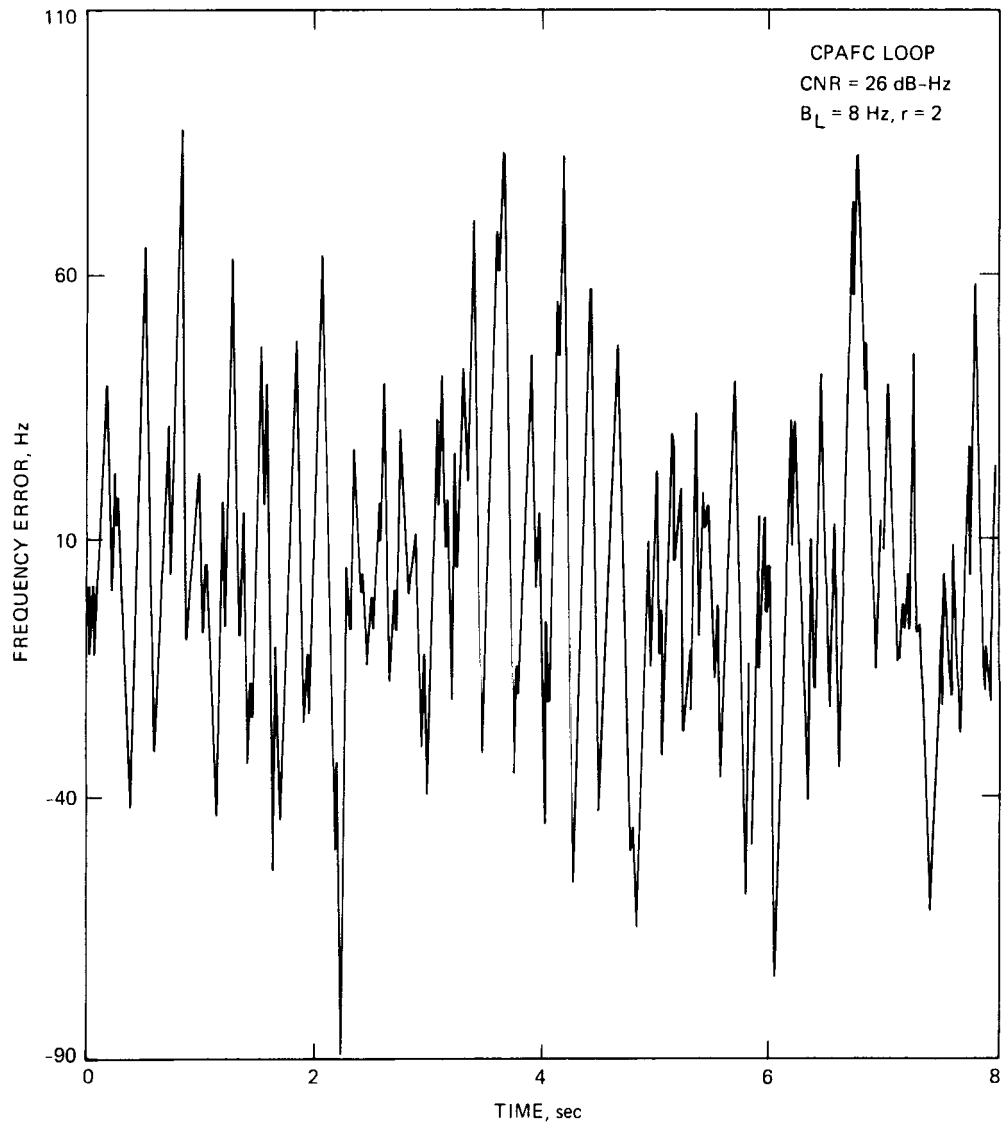

Figure 11. Instantaneous Frequency Error as a Function of Time (CPAFC)

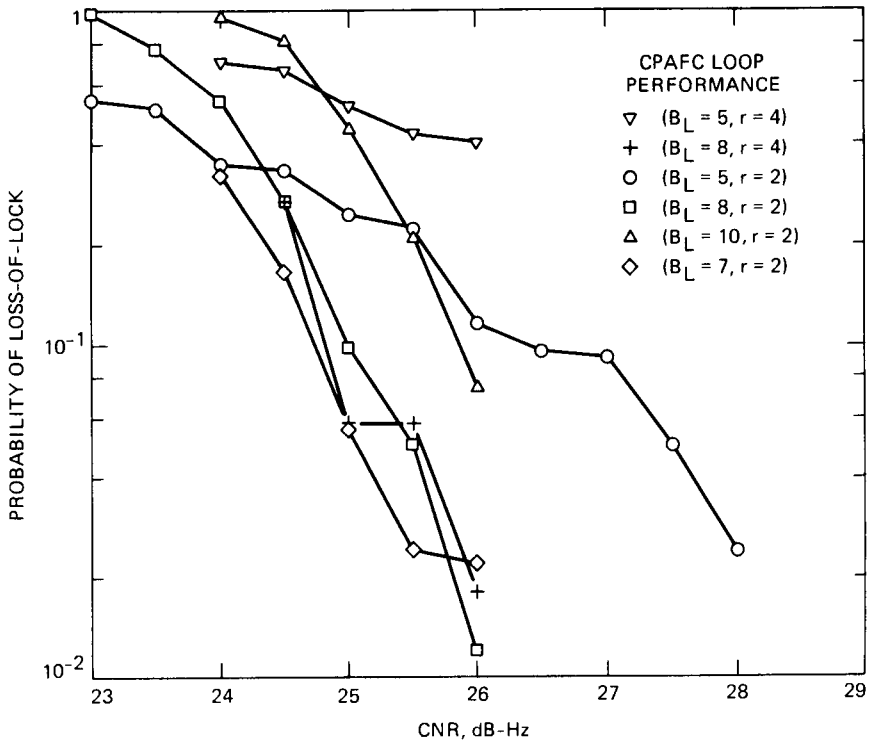

Figure 12(a). Estimated Loss-of-Lock Probabilities as Functions of CNR (CPAFC)

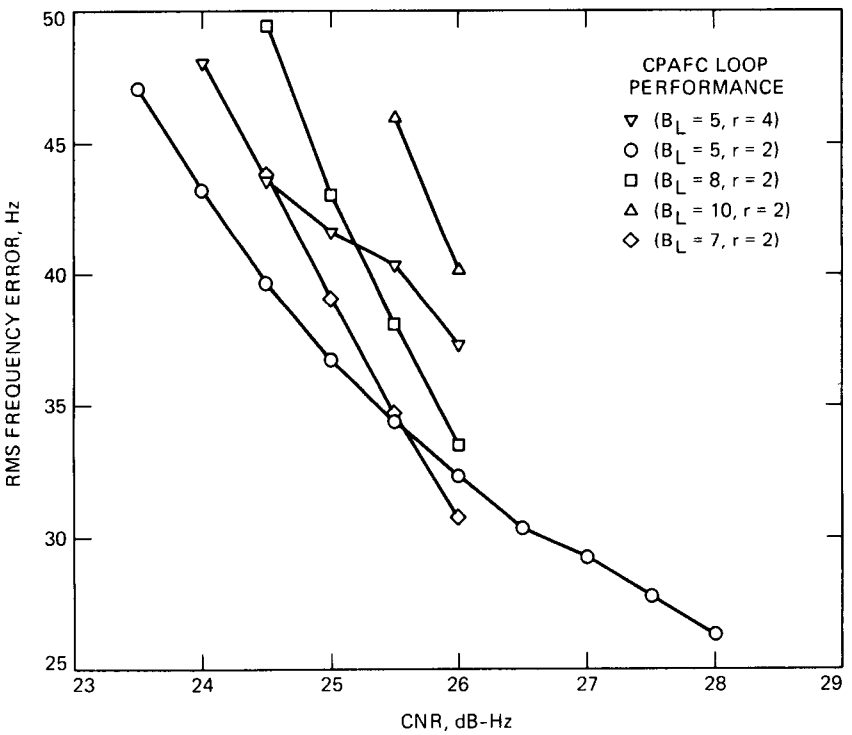

Figure 12(b). Estimated RMS Frequency Errors as Functions of CNR (CPAFC)

PHASE LOCKED LOOP (PLL) FREQUENCY ESTIMATOR

Frequency estimates can also be obtained from the traditional digital phase locked loop. The block diagram of this loop is basically the same as that of the AFC loop, with the discriminator and loop filter functions redefined. Because of the dynamics inherent in the common trajectory, a type-III loop was simulated since it can track linear frequency variations with zero steady-state error.

a. Phase Locked Loop Estimator Structure.

The loop filter was chosen to be an "impulse invariant transformation" filter (IIT) due to its simplicity and desirable performance characteristics. The filter transfer function [6] is

$$F(z) = G_1 + \frac{G_2}{1 - z^{-1}} + \frac{G_3}{(1 - z^{-1})^2} \tag{44}$$

where $G_1 = rd/T_s$, $G_2 = rd^2/T_s$, $G_3 = rkd^3/T_s$, and $d = 4B_L T_s(r - k)/r(r - k + 1)$. Here B_L is again the nominal loop bandwidth, used to define the parameter d. Note that a second-order loop filter and the third-order numerically controlled oscillator used in the simulation [6] yield a fifth-order digital loop. However, this loop behaves like a type-III analog loop. For the simulations, a sinusoidal phase detector characteristic was assumed. Frequency estimates were obtained from the phase samples via the difference equation

$$\hat{f}_n = \frac{\hat{\theta}_n - \hat{\theta}_{n-1}}{2\pi T_s} \quad \text{(Hz)} \tag{45}$$

where $\hat{\theta}_n$ denotes the phase estimate sample at time nT_s.

b. Estimator Performance.

For the parameter values defined above, we have from [6] that the steady-state phase error due to a constant jerk of magnitude J (m/sec^3) is

$$\theta_{ss} = \frac{\omega_c}{c} \frac{J_0 T_s^3}{rk} \left[\frac{r(r - k + 1)}{4B_L T_s (r - k)}\right]^3 \quad \text{(rad)} \tag{46}$$

while the phase error variance due to noise is

$$\sigma_\phi^2 \simeq \left(\frac{N_0}{A^2}\right) B_L \quad (\text{rad}^2) \tag{47}$$

The loop bandwidth should be chosen to minimize the sum of the estimation errors due to both trajectory and additive noise.

c. Simulation Results.

It was found by simulation that a nominal loop bandwidth of 43 Hz (r = 3, k = 0.5) minimized the probability of losing lock for our trajectory. For this bandwidth with J = 100 g/sec, Eqs. (51) and (52) yield θ_{ss} = 0.46 rad and σ_θ = 0.095 rad at a CNR of 26 dB-Hz. The simulations compare favorably with theory for two extreme cases, namely the case without thermal noise and the case without jerk. Estimates of the rms phase estimation error and the

frequency estimation error are shown in Figs. 13(a) and (b), respectively. Both estimation errors increase with decreasing CNR without much evidence of thresholding. However, we note from Fig. 13(c) that the probability of loss-of-lock exhibits a well-defined threshold around 26 dB-Hz.

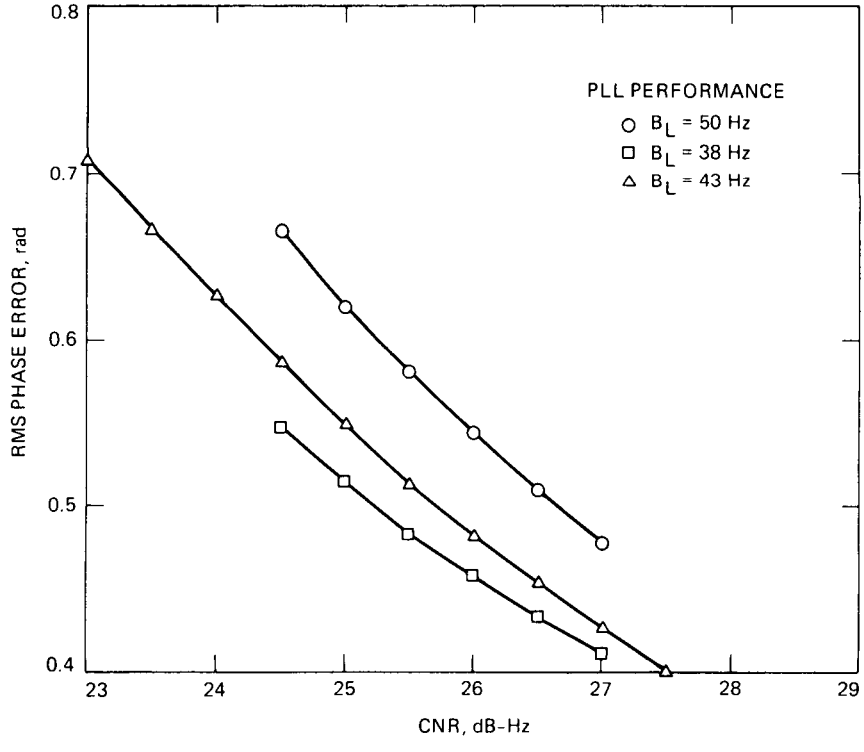

Figure 13(a). Estimated RMS Phase Errors as Functions of CNR (PLL)

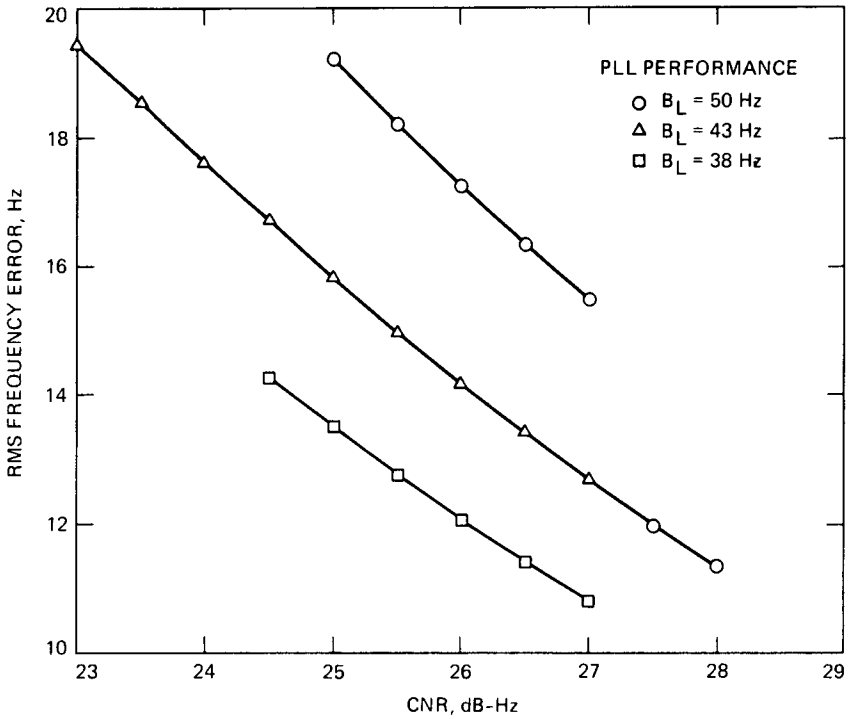

Figure 13(b). Estimated RMS Frequency Errors as Functions of CNR (PLL)

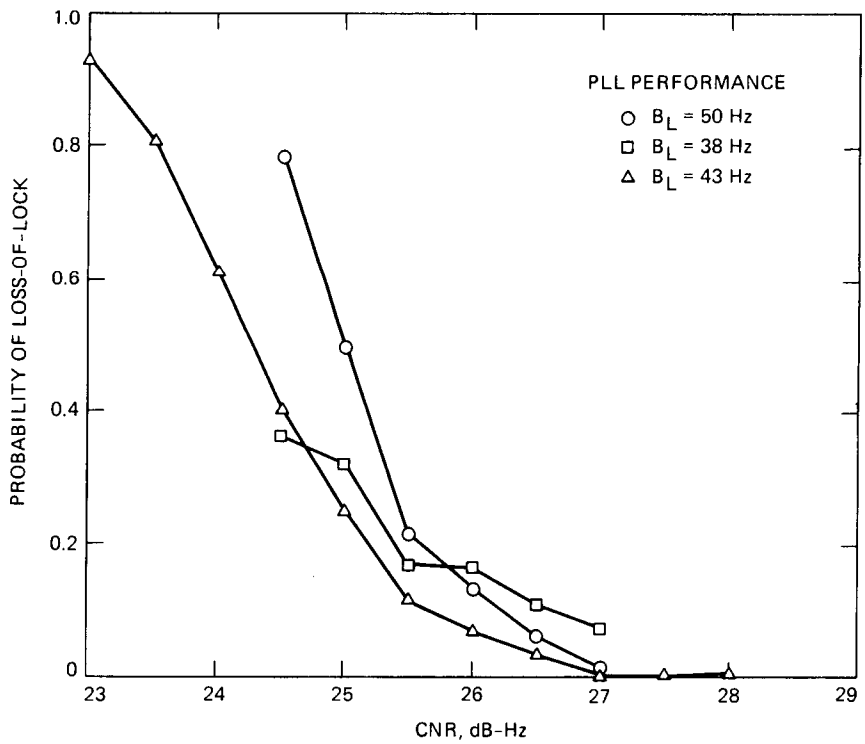

Figure 13(c). Estimated Loss-of-Lock Probabilities as Functions of CNR (PLL)

V. COMPARISON OF RESULTS

As mentioned in the introduction, our primary interest is to estimate the frequency of the incoming signal. Other signal parameters, such as phase or frequency rate are considered to be of secondary importance here. Some of the algorithms naturally provide estimates of secondary parameters in the process of estimating the primary ones. For example, the maximum likelihood algorithm estimates the rate-of-change of frequency, the phase locked loop derives frequency estimates from phase estimates, while the extended Kalman filter estimates all three parameters simultaneously. In the following paragraphs we compare the various algorithms on the basis of their ability to track a common frequency trajectory, while commenting on their ability to estimate the other parameters.

The loss-of-lock probability for each algorithm as a function of CNR is shown in Fig. 14(a). The parameter set that achieved the lowest threshold was selected in each case. Threshold is defined as the CNR at which the loss-of-lock probability for frequency estimation is 0.1. The approximate maximum likelihood estimator achieved the lowest threshold among the algorithms tested, namely 23 dB-Hz. The threshold for the extended Kalman filter was 24 dB-Hz, whereas the cross-product AFC loop and the phase-locked loop attained thresholds of 24.7 dB-Hz and 25.7 dB-Hz, respectively. The difference in thresholds is due to unequal sensitivity to severe dynamics among the various implementations.

The root-mean-squared (rms) frequency estimation errors are displayed in Fig. 14(b), again as functions of CNR. For each algorithm, the parameter set

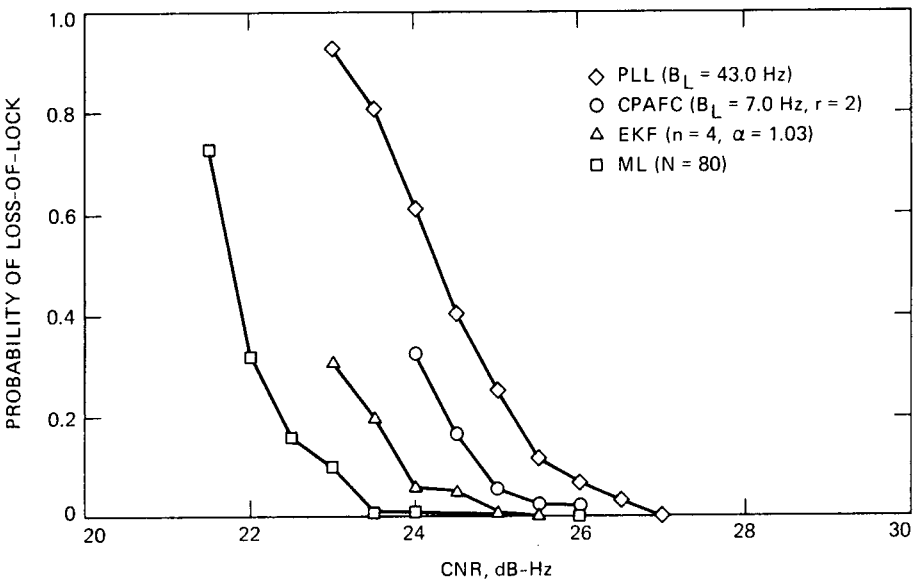

Figure 14(a). Comparison of the Four Estimators on the Basis of Loss-of-Lock Probabilities

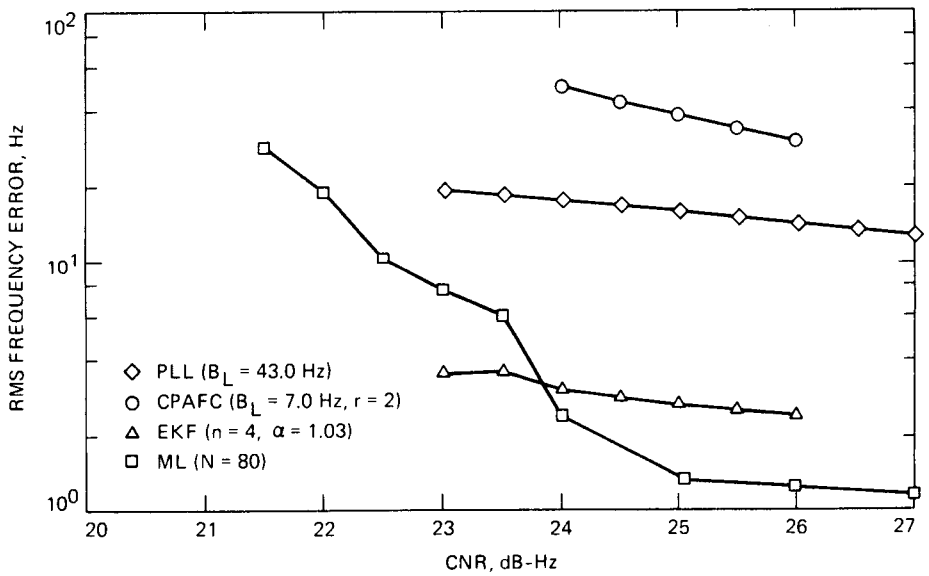

Figure 14(b). Comparison of the Four Estimators on the Basis of RMS Frequency Error

corresponding to minimum threshold was used. Note the sharp increase in rms estimation error for the ML algorithm near the loss-of-lock threshold. The rms estimation errors of the algorithms differ at threshold, which is typically the lowest CNR of interest. The EKF achieves roughly 3-Hz rms error at 24 dB-Hz, the PLL reaches 14-Hz rms at 25.7 dB-Hz, the ML yields 7-Hz rms at 23 dB-Hz, while the AFC algorithm operates with 40-Hz rms error at 24.7 dB-Hz. These values represent the smallest estimation errors each algorithm can achieve at threshold, below which loss-of-lock will frequently occur.

These algorithms should also be compared on the basis of operational comlexity, which we define as the average number of computations required per sample. The ML algorithm is the most complex, requiring the rapid computation of thirteen 256-point complex FFTs. The EKF requires approximately one order of magnitude fewer computations than the ML algorithm. The AFC and PLL implementations are the least complex, with the PLL algorithm requiring the fewest computations.

The relevant estimator attributes are summarized in Table I. The last column indicates increasing relative complexity, ranked from one to four. The other columns display threshold, rms frequency estimation error at 26 dB-Hz (well above threshold for most estimators), and the availability of phase and frequency rate estimates. For many applications, the choice of a suitable estimator algorithm can be based on these attributes.

Table I. Overall Comparison of the Four Frequency Estimators

Algorithm	Threshold (dB-Hz)	RMS Error (Hz) 23 dB-Hz	RMS Error (Hz) 26 dB-Hz	Phase Estimate	Frequency Rate Estimate	Complexity
ML	23.0	7	1	No	Yes	4
EKF	23.9	3.5	2.2	Yes	Yes	3
CPAFC	24.7	60	31	No	Yes	2
PLL	25.7	20	12	Yes	No	1

VI. SUMMARY AND CONCLUSIONS

In this paper, four different frequency estimation algorithms were presented and discussed. An approximate maximum likelihood algorithm, an extended Kalman filter, a cross-product AFC loop, and a phase locked loop were compared on the basis of tracking a common frequency trajectory that exhibits severe dynamics. The results are applicable to high-dynamic trajectories in general. The maximum likelihood approach was found to attain the lowest loss-of-lock threshold (23 dB-Hz), and also the lowest rms estimation errors above threshold. Although the performance of the extended Kalman filter was somewhat worse in both respects, it was able to operate with lower frequency estimation errors near threshold. The digital phase-locked loop performed well above threshold, but could not maintain lock reliably below about 26 dB-Hz. The threshold for the cross-product AFC loop was somewhat lower than for the phase-locked loop, but its estimation errors above threshold were the greatest of the four algorithms tested. Based on these simulations, we conclude that frequency estimates approaching the theoretical bound for known accelerations can be achieved in dynamic environments comparable to our simulated trajectory by the approximate ML and the EKF algorithms. Performance in terms of loss-of-lock probability and estimation error will generally depend on the severity of the dynamics encountered, and on the extent to which the system parameters can be matched to the temporal characteristics of the dynamic trajectory.

REFERENCES

1. W. Hurd, J. Statman, V. Vilnrotter, "High Dynamic GPS Receiver Using Maximum Likelihood Estimation and Frequency Tracking," IEEE Transactions on Aerospace and Electronic Systems, vol. AES-23, No. 4, July 1987.

2. D. Rife and R. Boorstyn, "Single-Tone Parameter Estimation from Discrete Observations," IEEE Transactions on Information Theory, vol. IT-20, No. 5, September 1974.

3. F. Costello, "An Adaptive Two-Dimensional Kalman Tracking Filter," IEEE Transactions on Aerospace and Electronic Systems, vol. AES-16, No. 6, November 1980.

4. B.D.O. Anderson and J.B. Moore, Optimal Filtering, Prentice Hall: Englewood Cliffs, New Jersey, 1979.

5. F.D. Natali, "AFC Tracking Algorithms," IEEE Transactions on Communications, vol. COM032, No. 8, August 1984.

6. S. Aguirre and W. Hurd, "Design and Performance of Sampled Data Loops for Subcarrier and Carrier Tracking," TDA Progress Report 42-79, Jet Propulsion Laboratory, Pasadena, California, pp. 81-95, November 15, 1984.

APPENDIX

DERIVATION OF CRAMER-RAO BOUNDS

The Cramer-Rao (CR) bounds on estimation error variance are derived for the case of a sinusoid of unknown frequency, frequency rate, and phase. We assume that the following in-phase and quadrature measurements are available:

$$\begin{aligned} r_1(k) &= A \sin(\theta_0 + \omega_0 t_k + \beta_0 t_k^2) + n_1(k) \triangleq s_1(k) + n_1(k) \\ r_2(k) &= A \cos(\theta_0 + \omega_0 t_k + \beta_0 t_k^2) + n_2(k) \triangleq s_2(k) + n_2(k) \\ t_k &= t_0 + kT = (n_0 + k)\, T \quad ; \quad k = 0, 1, \ldots N - 1 \end{aligned} \tag{A1}$$

where $n_1(k)$, $n_2(k)$ are components of the noise vector satisfying Eq. (31b). We wish to obtain CR bounds for the unbiased estimation of the unknown but constant parameters θ_0, ω_0, and β_0. Denoting the parameter vector $(\beta_0, \omega_0, \theta_0)^T$ by $\underline{\alpha}$, and the conditional probability density function of the observation (conditioned on $\underline{\alpha}$) by $f(\underline{R};\underline{\alpha})$, $\underline{R}(k) = \{\underline{r}(k),\ 0 \leq k \leq N - 1\}$, $\underline{r}(k) = [r_1(k), r_2(k)]^T$, and following the development in [2], the ij-th element of the Fisher information matrix J becomes

$$J_{ij} = E\left\{\frac{\partial}{\partial\alpha_i} f(\underline{R};\underline{\alpha})\ \frac{\partial}{\partial\alpha_j} f(\underline{R};\underline{\alpha})\right\} = \frac{1}{\sigma_n^2} \sum_{k=0}^{N-1} \left\{\frac{\partial s_1(k)}{\partial\alpha_i}\ \frac{\partial s_1(k)}{\partial\alpha_j} + \frac{\partial s_2(k)}{\partial\alpha_i}\ \frac{\partial s_2(k)}{\partial\alpha_j}\right\}$$

where $\alpha_1 = \beta_0$, $\alpha_2 = \omega_0$, $\alpha_3 = \theta_0$. After some straightforward computation, we obtain

$$J = \frac{A^2}{\sigma_n^2} \sum_{k=0}^{N-1} \begin{bmatrix} t_n^4 & t_n^3 & t_n^2 \\ t_n^3 & t_n^2 & t_n \\ t_n^2 & t_n & 1 \end{bmatrix} \tag{A2}$$

Letting

$$J_N \triangleq \frac{\sigma_n^2}{A^2} J = \begin{bmatrix} a & b & c \\ b & c & d \\ c & d & e \end{bmatrix} \tag{A3}$$

the elements of the matrix J_N may be expressed in terms of N and n_0 as

$$\begin{aligned} a &= T^4 \{n_0^4 N + 4n_0^3 P + 6n_0^2 Q + 4n_0 R + S\} \\ b &= T^3 \{n_0^3 N + 3n_0^2 P + 3n_0 Q + R\} \\ c &= T^2 \{n_0^2 N + 2n_0 P + Q\} \\ d &= T \{n_0 N + P\} \\ e &= P \end{aligned} \tag{A4}$$

where

$$P = \sum_{k=0}^{N-1} k = N(N-1)/2$$

$$Q = \sum_{k=0}^{N-1} k^2 = N(N-1)(2N-1)/6 \qquad \text{(A5)}$$

$$R = \sum_{k=0}^{N-1} k^3 = N^2(N-1)^2/4$$

$$S = \sum_{k=0}^{N-1} k^4 = N(N-1)(2N-1)(3N^2-3N-1)/30$$

The bound on the error variance of the estimate of α_i is then given by (σ^2/A^2) multiplied by the i-th diagonal element of J_N^{-1}. This matrix can be expressed as

$$J_N^{-1} = \frac{1}{|J_N|}\begin{bmatrix} (ce - d^2) & * & * \\ * & (ae - c^2) & * \\ * & * & (ac - b^2) \end{bmatrix} \qquad \text{(A6)}$$

with

$$|J_N| = a(ce - d^2) - b(be - cd) + c(bd - c^2)$$

Substituting Eqs. (A4) and (A5) into Eq. (A6) yields

$$ce - d^2 = \zeta_1 T^2$$

$$ae - c^2 = \{4n_0^2\zeta_1 + 4n_0\zeta_2 + \zeta_3\}\ T^4 \tag{A7}$$

$$ac - b^2 = \{n_0^4\zeta_1 + 2n_0^3\zeta_2 + n_0^2\zeta_4 + 2n_0\zeta_5 + \zeta_6\}\ T^6$$

The explicit expression for $|J_N|$ and various ζs can be obtained in terms of N as follows:

$$|J_N| = T^6N^3\ (N-1)^2\ (N^4 + 2N^3 - 3N^2 - 8N - 4)/2160 \tag{A8}$$

$$\zeta_1 = N^2\ (N^2 - 1)/12$$

$$\zeta_2 = N^2\ (N-1)^2\ (N+1)/12$$

$$\zeta_3 = N^2\ (N-1)\ (2N-1)\ (8N^2 - 3N - 11)/180$$

$$\zeta_4 = N^2\ (N-1)\ (7N^3 - 23N^2 - 18N - 8)/60 \tag{A9}$$

$$\zeta_5 = N^2\ (N-1)^2\ (2N^3 - 3N^2 - 3N + 2)/120$$

$$\zeta_6 = N^2\ (N-1)^2\ (81N^4 - 162N^3 + 105N^2 - 56N - 8)/240$$

The variance of the frequency estimate $\hat{f}_0 = \hat{\omega}_0/2\pi$, the parameter of greatest interest, then has the following bound

$$\mathrm{var}(\hat{f}_0) \geq (\nu_2 n_0^2 + \nu_1 n_0 + \nu_0)\ \frac{\sigma^2}{A^2T^2\Delta(2\pi)^2} \tag{A10}$$

where

$$\nu_2 = 4\zeta_1,\ \nu_1 = 4\zeta_2,\ \nu_0 = \zeta_3,\ \Delta = |J_N|/T^6$$

For the special case $n_0 = 0$,

$$\text{var}(\hat{f}_0) \geq \frac{\nu_0 \sigma^2}{A^2 T^2 \Delta (2\pi)^2} \tag{A11}$$

If N is so great that the highest-degree terms in N dominate in the expressions for ν_0 and Δ, then

$$\text{var}(\hat{f}_0) \geq \left(\frac{N_0}{A^2}\right) \frac{96}{T^3 N^3 (2\pi)^2} \tag{A12}$$

Again for $n_0 = 0$, the error bound for $\hat{\beta}_0$ is

$$\text{var}(\hat{\beta}_0) \geq \frac{N^2(N^2 - 1)}{12\Delta} \left(\frac{\sigma^2}{A^2 T^4}\right) \tag{A13}$$

which may be approximated for large N as

$$\text{var}(\hat{\beta}_0) \gtrsim \frac{180\sigma^2}{A^2 T^4 N^5} \tag{A14}$$

Noting that $\beta_0 = 2\omega_1$, with ω_1 the frequency derivative in rad/sec^2, and also that $(\sigma^2/A^2 T_s) = (N_0/2P_c T_s)$ where (P_c/N_0) is the received signal power-to-noise spectral density ratio, we obtain

$$\text{var}(\hat{\omega}_1) \gtrsim \frac{22}{T^5 N^5} \left(\frac{N_0}{P_c}\right) \tag{A15}$$

in units of $(Hz/sec)^2$. Comparison with the bound in Eq. (23) shows that the performance bound for estimating f_0 is a factor of 16 greater in the presence of an unknown frequency rate, than for the known (or zero frequency rate) case.

TECHNICAL REPORT STANDARD TITLE PAGE

1. Report No. 88-21	2. Government Accession No.	3. Recipient's Catalog No.
4. Title and Subtitle A Comparison of Frequency Estimation Techniques for High-Dynamic Trajectories		5. Report Date September 15, 1988 6. Performing Organization Code
7. Author(s) V. Vilnrotter, S. Hinedi, R. Kumar		8. Performing Organization Report No.
9. Performing Organization Name and Address JET PROPULSION LABORATORY California Institute of Technology 4800 Oak Grove Drive Pasadena, California 91109		10. Work Unit No. 11. Contract or Grant No. NAS7-918 13. Type of Report and Period Covered
12. Sponsoring Agency Name and Address NATIONAL AERONAUTICS AND SPACE ADMINISTRATION Washington, D.C. 20546		14. Sponsoring Agency Code

15. Supplementary Notes

16. Abstract This report presents a comparison of four different estimation techniques applied to the problem of continuously estimating the parameters of a sinusoidal Global Positioning System (GPS) signal, observed in the presence of additive noise, under extremely high-dynamic conditions. Frequency estimates are emphasized, although phase and/or frequency rate are also estimated by some of the algorithms. These parameters are related to the velocity, position, and acceleration of the maneuvering transmitter. Estimated performance at low carrier-to-noise ratios and high dynamics is investigated for the purpose of determining the useful operating range of an approximate maximum likelihood (ML) estimator, an extended Kalman filter (EKF), a cross-product automatic frequency control (CPAFC) loop, and a digital phase-locked loop (PPL). Numerical simulations are used to evaluate performance while tracking a common trajectory exhibiting high dynamics.

17. Key Words (Selected by Author(s))	18. Distribution Statement
Tracking, Navigation, Maximum Likelihood Estimator, Dynamic Frequency Estimation, High-Dynamic GPS, Extended Kalman Filter, Cross-Product Automatic Frequency Control loops, Phase-Locked Loops	Unclassified -- Unlimited

19. Security Classif. (of this report)	20. Security Classif. (of this page)	21. No. of Pages	22. Price
Unclassified	Unclassified	69	